GIS Center   FIU Libraries

2-2-2012

Consulting Services to Determine the Effectiveness of Vegetation Classification Using WorldView 2 Satellite Data for the Greater Everglades

Daniel Gann
GIS-RS Center, Florida International University, gannd@fiu.edu

Jennifer H. Richards
Department of Biological Sciences, Florida International University, richards@fiu.edu

Himadri Biswas
GIS-RS Center, Florida International University, hbiswas@fiu.edu

Follow this and additional works at: http://digitalcommons.fiu.edu/gis

Part of the Remote Sensing Commons

Daniel Gann, M.S.

Research Associate

GISRS-Center – Florida International University

11200 SW 8th St

Miami, FL 33199

305-348-1971; gannd@fiu.edu

Consulting Services to Determine the Effectiveness of Vegetation Classification Using WorldView 2 Satellite Data for the Greater Everglades

Synthesis Report: accepted 02/20/2012

Collaborative effort of Daniel Gann[1,2] , Dr. Jennifer Richards[2] , Himadri Biswas[1]

1) GISRS-Center FIU, 2) Department of Biological Sciences FIU

Table of Contents

Abstract

The purpose of this project was to evaluate the use of remote sensing 1) to detect and map Everglades wetland plant communities at different scales; and 2) to compare map products delineated and resampled at various scales with the intent to quantify and describe the quantitative and qualitative differences between such products. We evaluated data provided by Digital Globe's WorldView 2 (WV2) sensor with a spatial resolution of 2m and data from Landsat's Thematic and Enhanced Thematic Mapper (TM and ETM+) sensors with a spatial resolution of 30m. We were also interested in the comparability and scalability of products derived from these data sources. The adequacy of each data set to map wetland plant communities was evaluated utilizing two metrics: 1) model-based accuracy estimates of the classification procedures; and 2) design-based post-classification accuracy estimates of derived maps. The following four questions guided this research:

1) What is the overall and class-specific detection accuracy for Greater Everglades freshwater marsh plant communities from medium spectral and high spatial resolution (i.e., World View 2) and from medium spectral and medium spatial resolution (i.e., Landsat) satellite data?
2) How do overall and class-specific classification accuracies differ at different thematic hierarchical levels (i.e., detection at the plant community level vs. structural level) and different spatial resolutions (i.e., WV2 vs. Landsat and WV2 aggregated to Landsat spatial resolution)?
3) How do aggregation algorithms applied to high spatial resolution (detection) maps compare when aggregating to medium resolution maps using a morphological aggregation algorithm versus grid-based (arbitrary origin) majority rules? For the purpose of this project we were interested in two resolutions: 1) 30x30m, the pixel size of Landsat data; and 2) 50x50m, the grid cell size of visually interpreted vegetation maps provided by CERP 2004/2009.
4) How does the heterogeneity of grid-based maps aggregated by a simple majority rule compare to that of maps classified at the same grid-based resolution?

The research and mapping was done in two distinct regions of interest, the Tamiami Trail Bridge area, which included sub-regions north of Tamiami Trail and south of Tamiami Trail, and an area in the western part of Water Conservation Area 3A, which was comprised of two sub-areas (Fig. 1). To evaluate the suitability of remote sensing to detect plant communities in these landscapes, we established plant community classification schemata; acquired satellite data and performed atmospheric corrections; evaluated different classifiers; classified images using

the classifier with the highest model-based accuracy; and assessed post-classification accuracy. To investigate the scalability of plant community maps generated with remote sensing methods, we evaluated scaling using hierarchical thematic aggregation and grid-based vs. morphological spatial aggregation.

Our landscape classification scheme recognized three general scales. The coarsest thematic scale was the landscape morphology level; the next finer was the community structure level, which reflected the growth form of the dominant species; and the finest was the community class level, which reflected the dominant species. For each of the plant community classes we used the wet and dry season WV2 images to establish bi-seasonal phenological descriptors. To compare the WV2 images to Landsat data, we used Landsat TM and ETM+ data from dates comparable to the WV2 acquisition dates. Thus, we used data with spatial scales of 2m (WV2) and 30m (Landsat). The vegetation prediction was performed at the community class and community structural levels but not at the landscape morphology level.

We utilized the atmospherically corrected multi-spectral bi-seasonal images for both data sets, and in the case of WV2 data, we also included one local texture variable (variance for a 3x3 kernel). In classifying we tested the performance of two recursive partitioning algorithms: single tree (cTree) vs. multiple tree (randomForest) approaches. We also examined the performance of classification models that used bi-seasonal reflectance data versus a single dry or wet season only and, in the case of WV2 data, whether textural information added information useful in differentiating plant communities.

To compare class abundance changes when spatially aggregating high-resolution classified maps, we considered two spatial aggregation methods. The first method was a grid-based method where we aggregated the 2x2m resolution WV2 map to the 30x30m grid of the Landsat image and to the 50x50m grid utilized in the visual interpretation of aerial photography by CERP. In the second method we used a morphological aggregation algorithm based on the minimum mapping unit (MMU). This algorithm aggregated contiguous pixels in the same class based on the MMU, rather than by a grid with an arbitrary origin. Thus, pixels could be aggregated in non-square shapes.

Detection and Mapping Results

WV2 satellite images provide data with spatial, spectral and radiometric characteristics suitable for classifying Everglades wetland plant communities. Iterative data processing informed by field work and community class identification from contemporaneous aerial images resulted in maps that had high overall accuracy and Kappa estimates, especially when classified at the community structural level. Random forest classifier methods applied to the bi-seasonal and

4

textural data were able to classify plant communities and landscape patterns of conservation interest, such as wet prairies, ridges and sloughs, with high accuracy in both areas (100% for wet prairies, 99.5% for sloughs and 86.1 to 89.6% for tall graminoids, which are primarily sawgrass). In addition to accurately classifying vegetation, the WV2 data also provided fine-scale maps of plant communities with high spatial precision across the landscape that reflect the actual landscape morphology and class distributions. Landsat imagery preserved the general landscape morphology seen in the WV2 maps but lacked the degree of patchiness and community interspersion seen in the WV2 images, and individual patches had different sizes and shapes. Small classes with relatively isolated extents, such as the high heads of tree islands, also were lost in Landsat maps.

Scaling Results
Overall accuracy increased with scaling to lower thematic and spatial resolution. At the structural levels, model-based overall accuracies for hierarchically aggregated community classes for WV2 images were similar to accuracies for maps classified at the structural level. In general, accuracy was highest when pixels were classified at the community class level and then aggregated to the structural level versus classified at the community structure level. Classification at a lower spatial resolution caused loss of some community classes.

In both regions classifying vegetation at different scales changed the presence and abundance of community classes. When classifying at the community class level, decreasing the spatial resolution decreased class diversity; the same trend was present but not as marked at the structural level. In both areas, when aggregating WV2 pixels from 20 to 2500m^2 using the morphological aggregation method, fine-scale community class details and degree of interspersion were lost but overall community class shapes were preserved. The grid-based aggregation preserved the location and spatial distribution of large landscape classes, but the landscape shapes were pixelated and some classes were lost entirely.

Applications
A promising result of this study is the potential to use the methodology developed here to monitor landscape changes in response to management decisions. Because the WV2 maps preserved the shapes of landscape features at a high precision even when the minimum mapping unit was increased using the morphological aggregation algorithms rather than grid based methods, it should be possible to monitor changes in the shapes of these features.

The ability to map at a high resolution then aggregate to lower resolutions provides a way to quantify the effects of heterogeneous communities on the spectral signatures of coarser resolution satellite data.

Introduction

Detecting and monitoring wetland plant communities over large spatial extents and at multiple spatial and temporal resolutions depend on reliable, repeatable and inexpensive methods. The purpose of this project was to evaluate the use of remote sensing 1) to detect and map Everglades wetland plant communities at different scales; and 2) to compare map products delineated and resampled at various scales with the intent to quantify and describe the quantitative and qualitative differences between such products. Hence, the two main aspects of this study were "detection" and "scaling". To this end we evaluated data provided by Digital Globe's WorldView 2 (WV2) sensor with a spatial resolution of 2m and data from Landsat's Thematic and Enhanced Thematic Mapper (TM and ETM+) sensors with a spatial resolution of 30m. We were also interested in the comparability and scalability of products derived from these data sources. The adequacy of each data set to map wetland plant communities was evaluated utilizing two metrics: 1) model-based accuracy estimates of the classification procedures; and 2) design-based post-classification accuracy estimates of derived maps. The comparability and scalability of the maps was evaluated by comparing areal coverage changes of plant community abundances in maps of comparable scales and changes in class variability as resolution decreased.

Evaluation of the suitability of a mapping method for plant communities is driven by the intended purpose of the final product, which determines appropriate spatial resolution and thematic detail of the plant community classification scheme. In order to monitor community changes over short periods as a response to changed management practices, a definition of what constitutes plant community change needs to be established initially. Aspects of change to be considered are community compositional changes, structural changes (e.g., shrub to forest or short sawgrass to tall sawgrass), and spatial change through expansion or contraction of delineated landscape units. Thresholds at which change is considered significant need to be defined for all classes for each of these aspects of change. These thresholds and class boundary descriptions for each class can then be considered the class descriptions that separate community classes and are used to map plant communities at each time step.

For remotely sensed data plant community classification schemes and community class detection accuracies depend on the spatial detection resolution; this is limited by the sensor that acquires the data. Given this sensor resolution, the minimum mapping unit (MMU) for different maps can be expressed at multiples of the detection resolution at which the communities were originally mapped. Thus, detection resolution establishes the lower limit for map resolution, but it is possible and often desirable to map at coarser resolutions.

6

The first aspect for which suitability of a mapping method can be evaluated is the thematic accuracy of the map. The map is evaluated according to a pre-defined plant community classification scheme with thematic resolution relating to the number of classes. The two questions we were interested in with regard to plant community detection were:

1) What is the overall and class-specific detection accuracy for Greater Everglades (GE) freshwater marsh plant communities for the two distinct landscape formations of *Wet Prairie, Shrubland* mosaic and *Ridge, Slough, Tree Island* mosaic, from medium spectral and high spatial resolution (i.e., WV2) and from medium spectral and medium spatial resolution (i.e., Landsat) satellite data?

2) How do overall and class-specific classification accuracies differ at different spatial resolutions (i.e., WV2 vs. Landsat and WV2 aggregated to Landsat spatial resolution) and thematic hierarchical levels (i.e., detection at the plant community level vs. structural level?

A second aspect for which suitability of a mapping method can be evaluated is spatial precision. Spatial precision is of interest when attempting to capture contraction, expansion or disappearance of existing vegetation patches or the appearance of a new patch of a specific plant community. At a higher spatial resolution, the spatial extent of a patch boundary can be more precisely delineated, and smaller patches can be detected. High spatial resolution is required if minor changes of expansion or contraction are expected to be ecologically significant. For example, if a slough expansion of 10m is considered a significant change, then the spatial resolution to detect this expansion has to be 5m or less, allowing for a reasonable positional discrepancy among images of different dates, due to acquisition and registration procedures.

Scaling can occur with respect to both thematic accuracy and spatial precision. For example, it is possible to classify high spatial resolution data into detailed community classes in a hierarchical classification scheme, which, when aggregated to higher hierarchical levels, leads to greater spatial and thematic accuracy; this increase in accuracy results from misclassifications (confusions) within the same parent class being eliminated. Such an approach can be useful for detecting minor spatial expansion or contraction of major landscape units. Aggregation of smaller landscape units by combining all classes at the same hierarchical level of a classification scheme to the corresponding parent class does not change the map resolution or MMU, and patch boundary precision is maintained.

In contrast to thematic aggregation, spatial aggregation can be achieved in two ways: by increasing the size of the grid cells that are classified or by overlaying a grid of lower resolution over a high resolution map and assigning a new grid value based on some decision rule such as majority. In both cases the size of the MMU is increased, leading to a decrease in patch boundary precision. A second aggregation method would be a morphological aggregation of smaller landscape units to larger units, thus eliminating small patches by absorbing them into the surrounding matrix. This latter method eliminates patches smaller than the MMU while maintaining shapes of landscape features.

Depending on the thematic and spatial methods chosen, then, mapping plant communities for a specific region of interest (ROI) at a given time can lead to very different results. In this study we evaluated the effects of thematic aggregation within a classification hierarchy, as well as the effects of several ways to spatially aggregate landscape units.

In order to address scaling in the spatial and thematic domain, we posed two questions that guided us in the development of data processing algorithms and analysis methods:

3) How do aggregation algorithms applied to high spatial resolution (detection) maps compare when aggregating to medium resolution maps using a morphological MMU aggregation algorithm versus grid-based (arbitrary origin) majority rules?
For the purpose of this project we were interested in two resolutions: 1) 30x30m, the pixel size of Landsat data; and 2) 50x50m, the grid size of visually interpreted vegetation maps provided by CERP 2004/2009.

4) How does the heterogeneity of grid-based maps aggregated by a simple majority rule compare to that of maps classified at the same grid-based resolution?

This synthesis report summarizes our results and demonstrates the advantages and limitations of the methods and data that were evaluated. We will address the technical aspects of the image pre-processing, evaluation of the image classification procedures and the scaling methods in the Methods section, followed by a summary of major findings in the Results section. In the Discussion section we relate these findings to plant community detection and scaling in the context of plant community monitoring in the Greater Everglades.

Methods

The technical procedures were applied to two distinct regions of interest. The Tamiami Trail Bridge (TTB) area (Figure 1), which includes sub-regions NOrth of TAmiami Trail (NOTA) and SOuth of TAmiami Trail (SOTA,) can be characterized as peat wet prairies with mixes of tall graminoids dominated by *Cladium jamaicense* interspersed with patches of short graminoids dominated by *Rhynchospora tracyi, Eleocharis* species (including *E. cellulosa*, *E. elongata*, and *E. interstincta*) and abundant shrublands and small tree islands. The second region of interest was in the WEstern part of Water Conservation Area 3A (WE3A) and was comprised of sub-areas PSU2 and UASA (Figure 1). This landscape can be characterized as healthy ridge and slough mosaic with a regular alternating pattern of deeper sloughs populated by floating-leaved vegetation, such as *Nymphaea odorata,* and elevated ridges populated by *Cladium jamaicense;* tree islands with various shrub and tree species are interspersed among the ridges and sloughs.

In evaluating the suitability of remote sensing to detect plant communities of these landscapes, and to address questions 1 and 2 the procedural steps were:
1) Establishment of classification schema and class definitions for plant communities
2) Acquisition and atmospheric correction of satellite data
3) Model-based classifier evaluation and selection
4) Design-based post-classification accuracy assessment

To evaluate scalability of plant community maps generated with remote sensing methods, and to address questions 3 and 4 we performed:
5) Scaling method evaluation for
    a. Hierarchical thematic aggregation
    b. Grid-based spatial aggregation
    c. Morphological spatial aggregation algorithm

1) Establishment of Classification Schema and Class Definitions for Plant Communities

In order to investigate whether the spectral, radiometric and spatial characteristics of WV2 data were adequate to detect plant communities, we began the mapping process with the highest mapping resolution of 2m, as provided by the raw data, using a pixel-based supervised classification approach. Since a very fine plant community classification scheme, appropriate for 2m resolution, does not exist, we started to develop a new classification scheme,

considering existing plant community maps and their associated class schemata, as well as data accumulated through field work for this project. Plant community class definitions based on floristic and morphological criteria are common practice and are the basis for the classification systems used in the past for vegetation mapping in South Florida. We started with the identification of plant communities present in each of the two regions of interest. Available products were the stereoscopically derived 50x50m grid-based vegetation maps (CERP 2004 for NOTA) and (CERP 2009 for SOTA), which used the South Florida Natural Areas (SFNA) classification scheme (Rutchey, Schall et al. 2006), and a vector map delineated from 1995 aerial photographs (CERP 1995), which used the vegetation classification system for South Florida National Parks (SFNP) (Jones, Madden et al. 1999).

Both classification schemes (SFNA and SFNP) were designed for mapping at a minimum mapping unit (MMU) of 0.5ha for the grid-based maps and 0.25ha for the vector based maps. The intended final nominal MMU for our analysis was between 0.002ha and 0.004ha or 5 to 10 contiguous pixels of WV2 data. The increase in spatial resolution (larger scale) required a modification of the classification scheme, in order to accommodate classes that occurred at the higher spatial resolution but not at the MMU of the existing reference maps. Of special interest in this regard were those areas that were mapped as homogeneous plant communities in the reference maps (i.e., CERP 1995, 2004, 2009) that displayed a highly variable spectral reflectance pattern in the high resolution satellite images.

Our initial mapping attempt at 2x2m, therefore, required extensive field surveys that enabled us to establish a classification scheme that reflected the high spatial variability of the landscape, while also considering the frequency of occurrence across the landscape. If a classification system is too detailed, it is difficult to find enough training sites for each class, so misclassification becomes more likely and the information content of the map decreases for lack of generality.

Our field surveys revealed dominant species whose monotypic abundance across the landscape was high enough to be included at the lowest (most specific) community class level. The surveys also showed which interspersed mixes occurred frequently and how they could be grouped into higher level classes. Coupled with existing structural and floristic class characteristic descriptions, at the lowest level we differentiated classes of single species or mixes of species within their species structural level, i.e., the floating-leaved species structural category had six community classes defined by the dominant species present (Table 1). An exception to this hierarchy was short graminoid species mixed with broad leaved plants, which was a common mix in the wet prairies; this mix was classified by the combined species structural classes (i.e., GS_BL, Table 2). The initial list of dominant species that were recognized

at the community class level and all mixed classes are summarized in Table 1 and Table 2. Typically, classification schemes used in remote sensing are strictly hierarchical (Jensen 2005). Our high-resolution mapping approach with scaling to larger landscape units required us to create a fuzzy hierarchical classification scheme that allowed for aggregation and clustering based on relative abundances within a spatial matrix. This meant that at the smallest mapping unit, detection could occur at the species level, without consideration of the larger surrounding matrix. When the detection of communities at this level was concluded, spatial aggregation of the relative abundance of all other classes (matrix) determined the class at the new scale.

Following the SFNA and SFNP hierarchical plant community schemata (Jones, Madden et al. 1999; Rutchey, Schall et al. 2006) as closely as possible in order to maintain historical continuity and allow for comparisons, we combined their common features at the landscape level but added the flexibility of integrating relative abundance metrics into the classification scheme development at different scales (see Synthesis Discussion section). Our 3-level landscape classification scheme recognized three general scales. The coarsest scale was the landscape morphology. We recognized five morphological classes: Freshwater Marsh Slough (MFSL); Freshwater Marsh Wet Prairie (MFWP); Shrubland that could be embedded in either a Marsh (MS) or Swamp (SS) matrix; Swamp Forest (SF); and Swamp Woodland (SW) (Table 1, column 1). At the next finer thematic scale, we acknowledged five community structure classes: Slough (SL), composed of floating and submerged aquatic vegetation; Wet Prairie (WP), composed of a mix of short graminoids; Tall Graminoids (GT); Shrubs (S); and Trees (T) (Table 1, column 2). These structural classes were a reflection of the growth form of their dominant species and were therefore closely associated to the species-level dominant community classes (Table 1, column 3), which were composed of the dominant species abbreviated name (2 letter code Table 1, column 5) and the structural growth form of the species; in terms of species structural classes, we differentiated Broad-Leaved (BL), Floating-Leaved (FL), Short Graminoids (GS), Tall Graminoids (GT), Periphyton (P), Shrubs (S) and Trees (T) (Table 1, column 4).

Our field surveys indicated that although all of these classes exist in theory and probably are present in the GE region, their abundances varied greatly and not all occurred in our ROIs. Some classes were so rare, covering less than 0.1% of the landscape, that mapping them was meaningless. In other cases, even at the high resolution of 2x2m, we did not encounter pure classes with one dominant species but rather a mix of interspersed species. For these classes we introduced mixed classes. A complete list of community classes we attempted to map in each ROI is provided in Table 2, column 2, with associated community structural classes in column 1. The number of classes in each ROI was 17 and 13 for TTB and WE3A, respectively.

For each of the plant community classes we used the wet and dry season WV2 images to establish bi-seasonal phenological descriptors, considering different environmental scenarios in order to capture each class's spectral bi-seasonal response. These descriptors served to guide training pixel selection in order to cover as many as possible of the distinct phenological and spectral classes of each plant community. Additional work in this area could help to fine tune class-specific spectral boundary definitions. Class descriptions based on bi-seasonal phenological descriptors for plant communities, coupled with structural, floristic and density characteristics, were thus the starting points for establishing a plant community classification training data set.

2) Acquisition and Atmospheric Correction of Satellite Data

We acquired 4 WV2 multi-spectral and panchromatic images from Digital Globe; one wet and one dry season image for each of the two ROIs. Spatial resolution and spectral specification of the data are provided and summarized in Table 3. The wet season images of November 06th, 2010, were archived images, whereas the dry season May 5th, 2011, images were tasked by the Geographic Information Systems and Remote Sensing Center at FIU (GISRSC). Three cloud-free Landsat images were selected that corresponded to the November, 2010 (wet season) and May, 2011 (dry season) WV2 images. For the wet season, a Landsat 5 Thematic Mapper (TM) image dated December 25th, 2010, was selected. The dry season image for May could not be matched with a May Landsat 5 TM image, therefore we selected two Landsat 7 Enhanced Thematic Mapper Plus (ETM+) images dated March 07th and March 23rd, 2011. Spatial and spectral characteristics of TM and ETM+ data are provided in Table 4.

This study incorporated selection of training data for image classification from multi-temporal satellite images taken at different seasons, allowing us to incorporate class-specific phenological variability into our classification. Some of the factors upon which the quality of information derived from remotely sensed data depend are data quality, analysis techniques and interpretations, and numerous temporal and/or phenological considerations (Vogelmann, Helder et al. 2001). Changes in sensor characteristics, atmospheric conditions, solar angle, and sensor view angle affect the radiometric consistency of multi-temporal images (Chen, Vierling et al. 2005). In order to reduce these influences, radiometric corrections are performed to increase sensitivity to landscape change (Chen, Vierling et al. 2005). Therefore, all four WV2 images (wet and dry season TTB and wet and dry season WE3A) were radiometrically calibrated in order to eliminate exogenous differences as much as possible. Success of atmospheric correction was evaluated based on two methods: a relative comparison of reflectance values of pseudo-invariant features (PIF) between acquisition dates; and an absolute comparison to

reflectance of the PIFs with field collected spectra (limited to spectral range of spectrometer). We evaluated the sensitivity of atmospheric correction by applying different atmospheric models with variable visibilities (Tables 5, 6).

Absolute atmospheric correction was applied to the wet and dry season images, resulting in scaled surface reflectance values. Various atmospheric radiative transfer code models have been developed to determine effects of atmospheric scattering and absorption on satellite imagery. After removing these effects from each band and/or pixel in the imagery, the image is considered to be atmospherically corrected (Jensen 2005). We corrected our images utilizing ENVI's **F**ast **L**ine-of-sight **A**tmospheric **A**nalysis of **S**pectral **H**ypercubes (FLAASH) algorithm, which uses MODTRAN 4+ radiation transfer code solutions computed for each image and each pixel in the image and corrects images for atmospheric water vapor, oxygen, carbon dioxide, methane, ozone, and molecular and aerosol scattering (ITT_Visual_Information_Solutions 2009).

In order to determine the images on which the atmospheric correction worked best, pixels considered to be pseudo-invariant features (PIFs) were selected from atmospherically corrected wet and dry season images and were compared against each other. PIFs are characteristically spatially well-defined objects that are spectrally stable through time (Paolini, Grings et al. 2006). It was expected that after atmospheric correction, the PIFs would have very similar reflectance characteristics, and that those pixels would not differ for the wet and dry season. Corrected images that showed high differences in reflectance values were discarded and only similar reflectance images were quantitatively evaluated. For WV2 images, 91 pseudo-invariant pixels were randomly selected from water, asphalt, and concrete pixels and their spectral signatures were visually analyzed, followed by statistical procedures. Test of normality using Q-Q plots determined the appropriate statistical procedure (parametric or non-parametric) to test for differences. The differences in reflectance values of PIFs for each band (dry season subtracted from wet season) were not normally distributed. Therefore, non-parametric Wilcoxon Rank Sum tests were used to test for differences.   The Root Mean Square Error (RMSE) of differences for each matched pair of images was also determined. Images whose differences in reflectance values were not significant based on the Wilcoxon test were considered as candidates for the final selection based on RMSE estimates.   Atmospherically corrected images with lowest RMSE were determined to be best matches for wet and dry season images.

World View 2 Data
We selected atmospheric models from the standard MODTRAN atmospheric models based on latitude, month of year, and surface air temperature on the days the images were captured (see Table 5 for full list of evaluated models). The study area lies between 20°-30° N latitudes.

The wet and dry season images used in the study were captured in the months of November and May, respectively. The average temperature on the day the WorldView-2 images were captured was 57° F for the wet season and 80° F for dry season. Based on the above considerations, Mid-latitude Summer (MLS) and Tropical (TRP) atmospheric models were considered. For aerosol models, Maritime (Mari) and Tropospheric (Tropo) models were selected for WV2 images. The Maritime model represents the boundary layer over oceans or continents under a prevailing wind from the ocean. It is composed of two components, one from sea spray and another from rural continental aerosol that omits the largest particles. The Tropospheric model applies to calm, clear (visibility greater than 40 km) conditions over land. These atmospheric and aerosol models were applied in various combinations and the visibility parameter was varied between 40 and 100 km.

Landsat TM and ETM+ Data

The Landsat 7 ETM+ sensor developed a snag in the scan line corrector (SLC) and failed on May 31, 2003, with consequent data gaps in the acquired images. These data gaps can, however, be filled by using two or more images in which the fill scene should be captured as close as possible to the anniversary date of the primary SLC-off scene or should be at least from the same season (USGS 2010). Table 6 shows the models that were used to atmospherically correct the wet and dry season Landsat images. The average temperatures on the days the Landsat images were captured were 65° F and 68° F for wet and dry season images, respectively. Based on these temperatures, Mid-latitude Summer (MLS) and Tropical (TRP) atmospheric models were considered. These models were described above for the WV2 data. For aerosol models, Maritime and Rural (Rur) aerosol models were selected for the Landsat images. The Maritime model was described above for the WV2 data. The Rural model represents aerosols in areas not strongly affected by urban or industrial sources. The particle sizes are a blend of two distributions, one large and one small. These atmospheric and aerosol models were applied in various combinations and the visibility parameter was varied between 40 and 100 km.

Atmospheric Correction Results

WV2: A total of 128 sets of images were analyzed that included 16 atmospherically corrected dry season images that were compared against 8 atmospherically corrected wet season reference images. Only 9 sets of images showed no differences between them ($p > 0.05$). RMSE was high in all the bands and exceeded over 9% in all the bands. The first five bands varied between 11 to about 14%, and the last three bands varied by 11-13% in band 6, 10-11% in band 7 and 9-11% in band 8. Since the RMSEs were very close in each of the image comparisons, an additional test was performed, subtracting one corrected image from the reference image and comparing the total number of pixels that fell within +/-1% difference in reflectance in all the bands. The greater the number of such pixels, the better the match was considered. The number of pixels that were found in +/-1% difference in reflectance for these image

combinations are provided in Table 7. The dry season image with a MLS atmospheric model and a Tropo aerosol model with a visibility of 40 km (Dry_MLS_vis40_Tropo) had the highest number of pixels that fell within +/-1% difference in reflectance when compared to the wet season image with a MLS atmospheric and a Tropo aerosol model and a visibility of 100km (Wet_MLS_vis100_Tropo). We concluded that these two images were the best match and were consequently used for the bi-seasonal classification procedure.

Landsat: Prior to the seasonal comparison of corrected images, we had to fill the data gaps of the less cloudy image of Landsat 7 ETM+ from March 07th with the atmospherically corrected values of the March 23rd image. Before filling the data gaps, we evaluated the radiometric resemblance of the two corrected March images based on 47 PIFs, using the Wilcoxon Rank Sum test and RMSE. The p-values from the Wilcoxon Rank Sum test showed that the reflectance values from the atmospheric correction of the March 23rd image using different atmospheric and aerosol models and variable visibility did not differ from the primary image. The p-values were greater than 0.05 in all the bands of these images. The RMSE showed differences in reflectance of less than 2% in all the bands. Therefore, any of these three atmospherically corrected Landsat 7 ETM+ image was suitable to fill gaps in the primary reference image of March 7th. Since a tropical atmospheric model and rural aerosol model with a visibility of 100 km were used in the reference image, the atmospherically corrected March 23rd image with the same atmospheric models and visibility was selected.

Landsat 5 TM atmospherically corrected images were compared against the Landsat 7 ETM+ gap-filled image by selecting 20 PIFs and comparing reflectance values using the Wilcoxon Rank Sum test and RMSE. Wilcoxon Rank Sum tests indicated that there were no differences in the different atmospherically corrected Landsat TM images when compared against the Landsat 7 ETM+ gap-filled image. The p-values were above 0.05. RMSE values varied across all the bands in the images, with Wet_MLS_vis100_Rur being the image with lowest RMSE values in as many as three bands (Bands 4, 5, and 6). The visible bands (bands 1, 2, and 3) differed by 2.5, 3.5, and 4 per cent, respectively. The mid-infrared bands (Bands 5 and 6) also showed a low difference of 5.2 and 3.4 percent respectively. Therefore, we selected the Wet_MLS_vis100_Rur wet season image for plant community classification.

The evaluation of the absolute atmospheric correction results when compared to spectroradiometer data acquired in the field is still inconclusive because of spectrometer limitations in regard to range of wavelength overlap with both sensors, as well as spectrometer calibration difficulties.

3) Model-Based Classifier Evaluation and Selection

Detection of plant communities in the context of this report is defined as multivariate pattern recognition using supervised classification algorithms applied to remotely sensed data. Detection can be performed at various hierarchical levels of a classification scheme and it can occur at different spatial scales. We performed plant community detection on 2 data sets with spatial scales of 2m (WV2) and 30m (Landsat). The class prediction was performed at the community class and community structural level (Table 2). We utilized the atmospherically corrected multi-spectral bi-seasonal images, and in the case of WV2 data, we also included local texture variables derived from reflectance estimates using neighborhood statistics mean and variance for a 3x3 kernel (window size). Based on work performed in 2009 (Gann and Richards 2009), we decided to apply only recursive partitioning algorithms to detect plant communities, as these results outperformed all other classifiers in our previous work. The main reason for this is the large variability in bi-seasonal phenology of some classes, which leads to a large number of spectral classes per thematic class. The spectral signatures for each thematic class are not normally distributed in spectral reflectance space, and the number of spectral classes can be enormous. Recursive partitioning algorithms are very efficient and flexible when dealing with non-parametric data distributions and with the addition of new training samples as they become available.

We tested the performance of two recursive partitioning algorithms, single tree (cTree) vs. multiple tree (randomForest) approaches. Furthermore, we were interested in the performance of classification models that used bi-seasonal reflectance data versus a single dry or wet season only and, in the case of WV2 data, whether contextual spatial variability or textural information provided added information useful in differentiating plant communities. The classification performance was evaluated for community and structural class levels (Table 2). A complete list of models that were evaluated is given in Table 8.

For the single tree algorithm we employed the ctree function of the {party} package in R (R-project, CRAN), which utilizes a unified framework for conditional inference, or permutation tests (Strasser and Weber 1999; Hothorn, Hornik et al. 2006; Hothorn, Hornik et al. 2006). The multi-tree approach was tested using the randomForest function from the {randomForest} (Liaw and Wiener 2002) package in R, which implements Breiman's random forest algorithm (Breiman 2001; Breiman 2002). The packages we used for the reading, processing and analyzing of spatial vector, raster and table data in R, were {rgdal}, {raster}, {maptools}, and for the accuracy assessment component package {sampling} and {e1071}(Cohen 1960; Hubert and Arabie 1985).

Model-based accuracy assessment is determined from the analysis of the classified training data set. Evaluation of a confusion matrix derived from the classified training set has a large bias towards higher accuracies than expected for classification of unknown sample units. A cross-validation approach can reduce this bias. Both algorithms, ctree and randomForest, have built-in bootstrapping and cross-validation procedures to establish the classifier; a separate cross-validation test set to get an unbiased estimate of classifier model errors was therefore not necessary. The randomForest function constructs each tree with a different bootstrap sample and validates with the remaining data points, whereas the ctree function utilizes the cross-validation method to determine the pruning parameters of the tree, which avoids over-fitting the classifier model to the training set. Due to the non-randomness of the training sample selection, however, the actual map accuracy still needed to be assessed in a post-classification accuracy assessment based on random samples.

Training sample selection

Classifiers were constructed from training samples for which spectral reflectance values were extracted from the stacked image data cubes of wet and dry reflectance values and, if applicable, textural information. In the case of WV2 images, we started with a minimum of 20 samples per class and after each classification, visual inspection of the result determined obvious misclassifications of large patches. At that point, additional training samples were added for the class that was not recognized at that specific location. After each addition of a set of samples, the evaluation procedure was repeated. We went through 29 and 40 iterations for TTB and WE3A, respectively, with field reference sample collections between several iterations. For each field reference sample we determined the community class of the site at the GPS location (± 3m) and documented the vegetation at the site with a nadir photograph of the location and photographs in the 4 cardinal directions. This data was stored in a database that we used to further visually evaluate the plant community classes at and around each reference point.

In the case of Landsat images, we selected training samples for each class based on the resampled classification results of WV2 at the Landsat grid resolution (see scaling section, below). The sampling protocol included criteria for class dominance (purity) of a grid cell of > 85%. For each class 50 to 100 random samples were selected. If the number of sample candidates was less than 50, all samples were used.

4) Design-Based Post-classification Accuracy Assessment

Evaluation of the maps, which were generated with the classifier of highest overall accuracy estimated from the model-based evaluation, was performed with a design-based accuracy estimation. We conducted the post-classification accuracy assessment with a stratified random sampling design. The number of samples for each class was determined based on multinomial distribution probability theory. The number of samples per class was determined by the number of classes, the proportion of the most abundant class across the region of evaluation, the expected accuracy to be evaluated and the desired confidence of the estimate. Our goal was to test for a map accuracy of 90% with a 95% confidence.

For the 13 mapped classes of WE3A with greatest abundance of 47% for *Nymphaea odorata* (FLno), we sampled 54 samples per class for a total of 702 samples. For the 16 classes of TTB (OW was eliminated as it was only encountered and mapped at the airboat ramp) with greatest abundance of 30% for both *Cladium* (GTcj) and short Cladium (GTcjS), we sampled 39 samples per class for a total of 624 samples. It was prohibitive in terms of budget and time to ground reference each of these sites, so we assessed 36 and 56 of those samples at the community class level in the field for WE3A and TTB, respectively, limited by the sampling time frame of 1 airboat day in each ROI. Additional samples to the total number required were assessed using stereo-plotter technology with 2009 and 2011 aerial stereo imagery. Class specific numbers of community class field-assessed and stereo-plotter assessed community structure samples are provided in Table 9.

Since the reference data for the construction of the confusion matrix was collected for a small fraction of field samples, the accuracy for only some community classes could be established at this point and the confidence for the evaluated classes was very low. For the evaluation of community structure we determined the structural class membership using stereo-plotter technology. As in the case of the model-based evaluation, we calculated overall and class specific accuracies, as well as Kappa estimates and class specific omission and commission errors extracted from the confusion matrices.

5) Scaling Method Evaluation

For the comparison of class abundance changes when spatially aggregating high-resolution classified maps, we considered two spatial aggregation methods. The first method was a grid-based method where we aggregated the 2x2m resolution WV2 map to the 30x30m grid of the

Landsat image and to the 50x50m grid utilized in the visual interpretation of aerial photography by CERP.

The second method used a morphological aggregation algorithm based on MMU, which is determined by the number of contiguous pixels rather than by a grid with an arbitrary origin. Thus, pixels could be aggregated in non-square shapes. In order to preserve the shapes of larger landscape features at the structural level, we used this aggregation algorithm to develop a method that aggregated classes within the hierarchical level of community structure (Table 2). This meant that spatial aggregation occurred from consolidated classes at the structural level. Community classes within a homogenous structural patch were initially not aggregated in order to preserve the community class variability. For instance a periphyton patch (Pb) within a patch of mixed short graminoids (GSmix) would not be absorbed by the surrounding patch when aggregating at the community level. If the same patch was encountered within a patch of *Cladium* (GTcj), it was absorbed. In a second step, reclassification of the aggregated structural units eliminated the variability of the community class details, delivering a second map with only structural classes. In order to evaluate the heterogeneity and change in class abundances at the community class and structural levels, we aggregated the high-resolution maps at 20, 40, 400, 900 and 2500m^2. The latter two MMUs are comparable to Landsat and CERP map spatial resolutions, respectively. For the aggregation and generation of summary statistics we developed a python script in the arcpy environment of ArcGIS 10.

At each scale we evaluated the change in relative abundance of community classes and of the hierarchically aggregated structural classes. We also considered the number of classes lost due to the aggregation process.

Results

For the community class thematic level the overall model-based classification accuracy estimates in the two ROIs ranged from 79.7 to 90.9% for the WV2 images and 93.1 to 94.0% for the Landsat images (oaMod; Table 10). The model-based classification accuracy for the community structure thematic level ranged from 91.3 to 96.1% for WV2 images, while accuracy for images classified at the community class level but aggregated to the community structure level were 94.6% (TTB) and 96.1% (WE3A) (oaMod; Table 10). Landsat images classified at the

community class level but aggregated to the community structure level had 96.3% (WE3A) and 98.2% (TTB) model-based overall accuracy (oaMod; Table 10).

The design-based accuracies estimated for the WV2 community structure maps were 88.9% (WE3A) and 92.0% (TTB) (oaDes; Table 10). For Landsat the design-based community class accuracies were 73.6% (WE3A) and 68.9%, while accuracies for maps classified at the community class level but aggregated to the community structure were 85.1% (WE3A) and 82.5% (TTB) (oaDes; Table 10).

We achieved higher accuracies with the random forest algorithm than with cTree (e.g., mean cTree vs. mean rndFor in accuracy, oaMod; Table 10). Models using the bi-seasonal images performed better than the wet or dry season alone (e.g., wet and dry vs. bi in model-based overall accuracy by variable set; Table 10), and models using both spectral and textural information performed better than those using spectral data alone (e.g., wet, dry and bi vs. wetTxt, dryTxt and biTxt in model based overall accuracy by variable set; Table 10). Thus, the best model for plant community classification with WV2 imagery was one using the random forest algorithm and bi-seasonal spectral and textural data (Table 10). The best model for the Landsat images was similar although we did not use textural data for these images (Table 10).

Overall accuracy increased with scaling to lower thematic and spatial resolution. Thus, for all algorithms and models, the community structure thematic level had greater model-based overall accuracy and Kappa values than the community class thematic level, while at both thematic levels, Landsat imagery had higher model-based overall accuracy than WV2 imagery (Table 10), which in part can be attributed to the elimination of highly interspersed classes in the Landsat classification. The highest overall accuracy was achieved when higher resolution classifications were aggregated to the structural level (e.g., classAggStruc; Table 10). At the structural levels, model-based overall accuracies for hierarchically aggregated community classes for WV2 images were similar to accuracies for maps classified at the structural level (e.g., models for comStruc vs. classAggStruc; Table 10).

Detection TTB - Wet Prairie, Shrubland, Tree Island Mosaic

<u>WV2</u>
The model-based overall accuracy and Kappa for community classification in the TTB region of interest using the bi-seasonal WV2 images was 85.7 and 85.7%, respectively, for images classified at the community class level (Table 11), 94.6 and 91.7% for the community class level aggregated to the community structure level (Table 12), and 94.1 and 90.9% for the community

structure level (Table 13). The lower accuracy for the higher thematic resolution map came from several types of error. One was a sampling error; where there were not many samples of a particular class, any misclassification had a greater effect on accuracy, such as errors in the *Annona* forest class (Tag; Table 11). A second was an error in classifying species mixes in heterogeneous communities. An example of this was errors made in classifying the short graminoid (GSe, GSmix, and GSrt) communities, which consisted of mixtures of *Eleocharis* species, *Rhynchospora tracyi* and *Panicum hemitomon* (Table 11). The relatively high omission and commission error rates among these communities (up to 43%) indicated the difficulty in distinguishing among these mixes. The classes in the GS community, however, were rarely confused with other structural classes. Similarly, much of the error in the tall graminoid community classes came from misclassifications among tall and short sawgrass and the general sawgrass class (GTcj, GTcjS, GTcjT; Table 11). The accuracy for tall *Cladium* (GTcjT) of only 38% can be explained with the commission of almost 50% (28 of 60 samples) to the general *Cladium* class (Table 11). The selection of training samples was based solely on intensity of reflectance in the near-infrared rather than field measurements and the relative intensity of reflectance in that wavelength is a continuum reflecting density and height. No thresholds have been established for these height classes in sawgrass, therefore high confusion was anticipated.   As with the GS community, the sawgrass communities had relatively low levels of confusion with other community classes.

Accuracy was highest when pixels were classified at the community class level and then aggregated to the structural level versus classified at the community structure level, although model-based classification accuracy increased only slightly from 94 to 95% (oa(%); Table 12 vs. 13).   The lowest class specific accuracy at this level was 86.2% for the broad-leaved community (BL) when aggregated and 80.8% when classified at the structural level(Table 12,13). Highest accuracy was achieved for the wet prairie (WP) class with an overall accuracy of 97% for aggregated (Table 12) vs. 95.3% for classified at the structural level (Table 13).
The design-based accuracy estimates for the community structure level showed a 92.0% overall accuracy with a Kappa value of 89.3% (oaDes, kaDes; Table 10). Wet prairie (WP), broad-leaved (BL), tall graminoid (GT), and tree (T) were classified at high accuracies of 100, 98.2, 89.6 and 93.0%, respectively, with shrub (S) being the only class with a medium accuracy of 75.2% (Table 21).

Maps from WV2 imagery of the classified plant communities in the Tamiami Trail ROI reflected the shape of these landscape units and both the community heterogeneity and patchiness of this landscape (Figures 2, 3). The community structure map (Figure 3) preserved the morphology of the landscape units seen in the community class map (Figure 2).   The increased

accuracy of this map, however, came at the cost of decreased landscape unit diversity (Figure 2 compared to Figure 3).

<u>LANDSAT</u>

The model-based overall accuracy and Kappa estimate for TTB plant community classification with Landsat imagery using the bi-seasonal images was 94.0 and 93.0%, respectively, at the community class level (Table 14). At the lower spatial resolution of Landsat, some less common community classes (i.e., those that were not dominant with at least 85%) were excluded from the classification scheme. These classes were open water (OW), bayhead trees (TB), *Blechnum* in the broad-leaved class (BLbs), short graminoid *Eleocharis* spp. (GSe) in the wet prairie (WP), and tall graminoid *Cladium* tall (GTcjT) classes.

Similar to WV2 results, model-based accuracy was highest at 98.2% (oa(%); Table 15) when pixels were classified at the community class level and then aggregated to the structural level. Wet prairie (WP) was classified with the highest accuracy at 99.4% and broad-leaved (BL) with 93.3% at the lowest (Table 15).

The difficulty distinguishing among community classes at the 30x30m pixel resolution was seen in classification of the short graminoid *Rhynchospora tracyi* (GSrt) community class; we found only 5 pixels of this class that were pure enough to be included in the training set, and they were all misclassified (Table 14). Once the more detailed thematic classes were aggregated at the community structure level, the overall accuracy increased to 98.2% with a Kappa value of 97.4% (Table 15 vs. Table 14).

Maps of the TTB ROI derived from the Landsat imagery preserve the general landscape morphology seen in the WV2 maps (Figures 4, 5). The Landsat maps, however, lack the degree of patchiness and community interspersion seen in the WV2 images, and individual patches have different sizes and shapes (Figure 4 vs. Figure 2, Figure 5 vs. Figure 3). For example, there are fewer wet prairie patches (GS or BL classes at the community class level, WP at the structural level) in the western third of the Landsat maps as compared to the WV2 maps, and these patches are less interconnected, while there are larger and more interconnected patches in the eastern two-thirds of the Landsat maps as compared to the WV2 maps (Figures 4 and 5 vs. Figures 2 and 3).

Small classes with relatively isolated extents, such as the high heads of tree islands, also were lost in the Landsat maps, e.g., the loss of the entire bayhead class (TB) for TTB (Figure 4). This circumstance will change if the ROI is extended to larger areas with sufficient representation of

such small classes if they exist as homogeneous areas across the landscape and with patches large enough to be captured at 30x30m resolution.

Detection WE3A - Ridge, Slough, Tree Island Mosaic

<u>WV2</u>

The model-based overall accuracy and Kappa estimate for community classification in the WE3A region of interest using the bi-seasonal WV2 images was 90.9 and 88.7%, respectively, for WV2 images classified at the community class level (Table 16), 96.5 and 94.1% for the community class level aggregated to the community structure level (Table 17), and 96.1 and 93.3% for WV2 images classified at the community structure level (Table 18). At the community class level of classification, the WE3A ROI lacked the short graminoid (GS) wet prairie community classes and the short sawgrass (GTcjS) community class, which increased classification accuracy within the wet prairie and sawgrass classes (Table 16). This region had slough communities, which were not found in the TTB ROI, and had a greater number of distinguishable broad-leaved communities (Table 16). The floating-leaved *Nymphaea odorata* community class (FLno) and the sawgrass community class (GTcj) had the highest classification accuracies (94.6% and 94.6%, respectively) of any of the WE3A communities (Table 16). As with the TTB ROI, less frequent community classes tended to have lower accuracies (e.g., the *Peltandra virginica* broad-leaved community class, BLpv).

As with the TTB classifications at different scales, the WV2 imagery classified at the community class level then aggregated to the structural level had higher overall accuracy and Kappa estimates than the same imagery classified at the structural level, and, like the TTB case, the differences were small (Table 17 vs. Table 18).

Design-based accuracy estimates for the community structure classes (Table 22) showed similar results to those in the TTB ROI. An 88.9% overall accuracy with a Kappa of 85.6% was achieved with a very high individual class accuracy for slough (SL) of 99.5% , and high accuracies for broad-leaved (BL), tall graminoid (GT), and shrub (S) classes of 83.7.2, 86.1 and 85.4%, respectively; only the tree (T) class (79.1%) fell below 80% (Table 22).

The map generated from the community class classification of the WV2 images shows the typical ridge-slough-tree island landscape found in this area of WCA 3A (Figure 6). The maps reflect the ridge and slough orientation and spacing, as well as the head and tail structure of the tree islands. These maps also show the shape and plant community diversity of these landscape features. Of particular interest are the small patches of both sawgrass and broad-

leaved plants found in the slough areas and the small patches of broad-leaved plants and shrubs, especially willow, found in the sawgrass ridges (Figure 6). This map also gives a unique view of the distribution of the floating periphyton.

The map of WE3A vegetation classified at the community class level and aggregated to the structural level preserved the morphology and patchiness of the landscape, including the small patches of sawgrass and broad-leaved plants in the slough, the broad-leaved plants and shrubs in the ridges, and the trees in the tree island heads (Figure 7). As with the TTB ROI, the increased accuracy of this map came with decreased class diversity (Figure 7 vs. Figure 6).

LANDSAT
The model-based overall accuracy and Kappa estimate for WE3A plant community classification with Landsat imagery using the bi-seasonal images was 93.1 and 91.2%, respectively, at the community class level (Table 19). Classes lost at the coarser spatial scale, as compared to the WV2 community class map (Table 16), included the floating-leaved *Utricularia* spp. class (FLu) and the tall graminoid cattail and tall sawgrass classes (GTt, GTcjT). As with the TTB ROI, classes with few training samples had low levels of accuracy (e.g., the open water (_OW), broad-leaved *Peltandra virginica* (BLpv) and bayhead tree (TB) classes, with 5, 3 and 2 pixels and 40, 67 and 0% accuracies, respectively) (Table 19).

When the Landsat images were classified at the community class level then aggregated to the structural level, the model-based overall accuracy and Kappa estimate increased to 96.3 and 94.7% (Table 20). These levels were comparable to the WV2 classifications at the same thematic scale (Table 20 compared to Table 17, 18).

As with the TTB ROI, maps of the WE3A ROI made from the Landsat images preserve the general landscape morphology seen in the WV2 maps, but lack the patchiness and detail (Figures 8, 9). The general shape and orientation of the ridges and sloughs is reflected in these maps, as is the distribution of woody communities on the tree islands. The diversity of community classes occurring in the sloughs, ridges, and tree island tails, however, is largely lost (Figure 8 vs. Figure 6 and Figure 9 vs. Figure 7). The spatial extent of some communities is greater in the Landsat maps (e.g., the floating periphyton community, Figure 8 vs. Figure 6), while abundance decreases for other community classes (e.g., the tree community, Figure 9 vs. Figure 7).

Scaling TTB - Wet Prairie, Shrubland, Tree Island Mosaic

Area north of the Tamiami Trail Bridge (NOTA): Classifying vegetation in southern WCA 3B at different scales changed the presence and abundance of community classes (Figures 2, 4, 5, Table 23). When classifying at the community class level, decreasing the spatial resolution decreased class diversity (Table 23). For this level, increasing the MMU from 1, 5 or 10 pixels (4, 20, or 40m^2) to 225 pixels (900m^2) decreased the number of classes mapped from 17 to 15 and 14 (WV2 images). Maps created from the Landsat images (900m^2 pixels) had even fewer classes (12). Similarly, maps from WV2 images aggregated to 50x50m (2500m^2), which is the grid size for the CERP maps, had 12 or 14 classes (Table 23). The lost classes were ones that were relatively rare or that had very dispersed small patches in the higher resolution maps.

Differences in class abundances among the WV2-derived maps were minor when scaling at the community class level from 4 to 400m^2 MMU (1 to 100 pixels) (comClass; Table 23). As the MMU increased to 900m^2, the greatest changes in abundance occurred in the sawgrass classes. Abundance of sawgrass classes (GTcj, GTcjS and GTcjT) increased at and above 900m^2, ranging from 67.8% (mmu900 and ls; Table 23) to 73% (grd2500; Table 23), as compared to 64.6% for sawgrass classes found in the map classified at the 4m^2 resolution (wv2; Table 23). Although the grid-based 900m^2 map had more sawgrass (GTcj) than the morphologically aggregated map at the same scale (48.8% vs. 43.7%), this difference was partially offset by the grid-based map having less short sawgrass (GTcjS). The total amount of sawgrass in the two maps was 69.9% (grid-based map) and 67.8% (morphological-aggregation map). Using a grid-based aggregation method made a greater difference at the 2500m^2 resolution, where the mmu2500 map had 69.1% sawgrass and the grd2500 map had 73.0% sawgrass (Table 23).

Similar trends in both community diversity and community abundance were seen when aggregating at the structural level (comStruc; Table 23). Rare classes were lost with decreased spatial resolution, although this trend was less marked than at the higher thematic resolution because there were fewer classes overall. The tall graminoid class (GT), which is composed primarily of sawgrass classes, increased in abundance by almost 7% when aggregating to morphological and grid-based 2500m^2 from the wv2 value, while the wet prairie class (WP) decreased in abundance 4 – 6% for morphological or grid-based 2500m^2 spatial resolution as compared to the wv2 value (Table 23). The method of pixel aggregation had little effect on class abundance at the structural level (mmu900 vs. grd900 and mmu2500 vs. grd2500; Table 23).

The effects of decreased resolution and of morphological vs. grid-based aggregation in the NOTA ROI are compared visually in Figure 10. Details are lost but overall community class

shapes are preserved in aggregating WV2 pixels from 20 to 2500m^2 using the morphological aggregation method (Figure 10, top four panels). The grid-based aggregation preserves the location and spatial distribution of large landscape classes, but the landscape shapes are pixelated and some classes are lost entirely (Figure 10, bottom two panels).

Area south of the Tamiami Trail Bridge (SOTA): As in southern WCA 3B (NOTA), vegetation classes in Everglades National Park south of the Tamiami Trail Bridge (SOTA) decreased in diversity and changed in abundance with decreasing spatial resolution (Figures 2, 4, 5, Table 24). Increased aggregation of the WV2 pixels at the community class level resulted in increased abundance of sawgrass classes (GTcj, GTcjS and GTcjT) from 61.2% at the 4m^2 resolution to 70.4% at the grid-based 2500m^2 resolution and decreased abundance of wet prairie classes (GS and Pb classes) from 16.6% to 8.9% (Table 24). At the community class level, morphological vs. grid-based aggregation had small effects at 900m^2 and 2500m^2 MMU (Table 24). Although the Landsat map had approximately half the amount of sawgrass (GTcj) as the WV2 maps at a similar spatial resolution, this decrease was partially balanced by an increase in the amount of short sawgrass (GTcjS; the overall amounts of sawgrass in these maps was 65.5% (mmu900), 68.2% (grd900), and 58.9% (ls) (Table 24). Changes in class abundance with decreased spatial resolution at the structural level paralleled those at the community class level, with the tall graminoid class (GT) increasing in abundance and the WP class decreasing (Table 24).

Across all levels of aggregation, the sawgrass classes in SOTA were slightly less abundant than those in NOTA (61.2% vs. 64.6% at 4m^2 resolution and 70.4% vs. 73% at the 2500m^2 grid resolution), but the short sawgrass class (GTcjS) was approximately twice as abundant in SOTA, while the sawgrass class (GTcj) was correspondingly reduced (Table 23 vs. Table 24). The wet prairie classes were more abundant in NOTA, while the shrub classes, especially the willow class (Ssc), were more abundant in SOTA. The cattail class (GTt) was close to twice as abundant in SOTA as compared to NOTA (Table 23 vs. Table 24).

The effects of decreased resolution and of morphological vs. grid-based aggregation in the SOTA ROI are compared visually in Figure 11. As in the NOTA ROI, the fine-scale community class details and degree of interspersion are lost in aggregating from 20 to 2500m^2, but overall community class shapes and boundaries are retained (Figure 11, top four panels). The grid-based aggregation preserves the location and spatial distribution of large landscape classes, but the landscape shapes are pixelated and some classes are lost entirely (Figure 11, bottom two panels).

Scaling WE3A - Ridge, Slough, Tree Island Mosaic

Spatial scaling had less effect on vegetation class diversity and abundance in the maps for WE3A as compare to the TTB ROI, although the trends of decreased diversity and increased abundance of common classes were seen at the community class level (Figures 6, 8, 9, Table 25). Maps at the 4 to 900m^2 resolution from the community class level had very similar class abundances for the morphologically aggregated maps (Table 25). The 900m^2 grid-aggregated map showed decreased percentages of less common classes and increased percentages of more common classes (Table 25). As was seen for the SOTA map, the Landsat images had decreased abundance of the most common class, which in this case was the water lily slough class (FLno), but this was balanced by an increased abundance of the floating periphyton slough class (_Pf), so the overall slough class percentage was only slightly less at the 900m^2 resolution (57.2% for mmu900 and grd900 vs. 56.1% for ls, Table 25). The Landsat-derived map had the lowest class diversity (10 classes) of any of the community class maps.

The communities most affected by scaling in the WE3A maps were the broad-leaved communities (BLbs, BLmix, and BLpv), although these classes formed only 3 to 8% of the landscape (Table 25); the broad-leaved classes decreased in abundance with decreased spatial resolution, but were much more common in the Landsat-derived map than in the WV2 aggregated maps at the same resolution (ls vs. mmu900 and grd900, Table 25). Decreased spatial resolution had no effect on diversity at the structural class level and minor effects on class abundances (Table 25).

The WE3A landscape was very different from the TTB landscape both in the distribution of classes on the landscape and in class composition (Figures 6-9, Table 25 vs. Figures 2-5, Tables 23 and 24). WE3A lacked the wet prairie communities found in the TTB area and had abundant slough community classes, which were mostly absent in the TTB area. Sawgrass classes were present but not as abundant as in the TTB area, and the short sawgrass class (GTs) was lacking (Table 25).

The effects of scaling and morphological vs. grid-based aggregation in the WE3A ROI are compared visually in Figure 12. As in the TTB ROI, fine-scale details and some community classes are lost with aggregation from 20 to 2500m^2, but the landscape morphology and community adjacency are retained (Figure 12, top four panels). Grid-based aggregation retains the general landscape shapes and general relations of major community classes, although orientation of the pattern becomes skewed (Figure 12, bottom two panels). In addition, less common classes are lost, as is the patchiness and interspersion of communities.

Synthesis Discussion

WV2 satellite images provide data with spatial, spectral and radiometric characteristics suitable for classifying Everglades wetland plant communities. Iterative data processing informed by field work and community class identification from contemporaneous aerial images resulted in maps that had high overall accuracy and Kappa estimates, especially when classified at the community structural level. Random forest classifier methods applied to the bi-seasonal and textural data were able to classify plant communities and landscape patterns of conservation interest, such as wet prairies, ridges and sloughs, with high accuracy (100% for wet prairies, 99.5% for sloughs and 86.1 to 89.6% for tall graminoids, which are primarily sawgrass). In addition to accurately classifying vegetation, the data also provided fine-scale maps of plant communities with high spatial precision across the landscape that reflect the actual landscape morphology and class distributions.

These maps provide a new image and greater understanding of plant community patchiness and interspersion that needs to be incorporated into our thinking about how communities might change under different restoration scenarios. For example, discussions of ridge and slough structure tend to consider ridges as largely homogeneous sawgrass strands and sloughs as dominated by water lily species and periphyton (Larsen, Harvey et al. 2007; Larsen and Harvey 2010; Watts, Cohen et al. 2010; Cohen, Watts et al. 2011; McVoy, Said et al. 2011). In many parts of the Everglades ridge and slough ecosystem, ridges have expanded into the slough, erasing the longitudinal patterning of the landscape and increasing sawgrass abundance. Models for how this expansion has occurred have concentrated on expansion of existing ridges (Larsen, Harvey et al. 2007; Larsen and Harvey 2010; Watts, Cohen et al. 2010; Cohen, Watts et al. 2011). Understanding that sloughs are seeded with small sawgrass patches, as our maps show, suggests that expansion and coalescence of these patches may also be important in slough in-filling.

Being able to map vegetation at a finer scale also allow for more accurate estimations of community abundances and for flexibility in hierarchical aggregation (e.g., it would be possible to maintain *Typha* as a separate structural class from all other tall graminoids when aggregating to coarser scales). The increased accuracy in community abundance estimation was seen in the results of aggregating the WV2 maps to coarser resolutions. When spatial aggregation was done at our most detailed thematic level (the community class level), the percentage of common classes increased, while the less common classes decreased; this effect was visible in the maps, was quantifiable, and was apparent when the 30x30m Landsat data was used to classify and map vegetation in the same ROIs. This scaling effect is a possible explanation for

the high abundances of sawgrass marsh in the CERP 2004 map for NOTA (76.3%) and 2009 map SOTA (76.0%), as opposed to 65 to 61% sawgrass (Tables 23 and 24; GT classes minus *Typha*) in our higher resolution maps in the same areas. Scaling effects may also explain the complete lack of wet prairie or open marsh communities in the SOTA region of the CERP 2009 Northern Everglades map, as compared to 16.6% in our maps (Table 24).

Another very promising result of this study is the potential to use this methodology to monitor landscape changes in response to management decisions. Because the WV2 maps preserved the shapes of landscape features at a high precision even when the minimum mapping unit was increased using the morphological aggregation algorithms rather than grid based methods, it should be possible to monitor changes in the shapes of these features. For example, the ridge and slough landscape features of WE3A are very different from the landscape features in the wet prairies, as seen in the TTB ROI. A change in structure of these landscapes could be evaluated by comparing landscape metrics over time (Watts, Cohen et al. 2010; Nungesser 2011). If landscape features change through expansion or contraction, then relatively small changes could be detected, since edges and feature shapes in the WV2-derived maps have much higher precision than features based on large grid cells (e.g., Figures 10-12). Alternatively, if environmental changes affect small vegetation patches before large vegetation patches, then such changes could also be detected in the higher resolution WV2 maps, but would be completely missed in maps with coarser resolution. If strategically located monitoring sites representative of the larger landscape heterogeneity, such as the CERP primary sampling units (PSUs), were assessed at annual to bi-annual temporal resolution, then monitoring their development at high resolution could provide good feedback on vegetation responses to changed management practices in a relatively short time. As demonstrated in this study, the digital image processing and digital mapping procedures using remote sensing and GIS techniques makes such monitoring both possible and affordable.

Despite the good results obtained in this study, several issues need to be addressed to make scaling of different map products possible and to make results comparable and more meaningful in the context of landscape vegetation monitoring at different scales. Classification schemes need to be developed for different scales. Higher level landscape units of larger size are more heterogeneous; vegetation classes at these levels will make more sense if they are defined by a full matrix of class abundances rather than by maintaining the classes frequently encountered at smaller mapping units. For example, a tree can be defined by height and diameter at breast height, and at a 2m resolution, individual trees can be mapped at the species level, if they are spectrally detectable and differentiable from other classes. The individual tree could be a single individual within a grassland matrix or a member of a forest or, if tree density is not high enough, a woodland. Thus, the context in which the tree occurs

determines class membership of the tree pixel at the larger landscape units. The appropriate classification scheme for a specific MMU or scale is therefore driven by the relative abundance of dominant species and their pattern of interspersion across the landscape. Spatial aggregation methods need to take into consideration frequency distributions of relative class abundances across the landscape.

Our aggregation exercise demonstrates the reason for a scale-specific classification scheme approach. When the WV2 community classes classified at 4m^2 were aggregated to the Landsat grid size of 900m^2, they produced a relative distribution of classes present within each grid cell. A majority classifier that assigns the dominant class of the relative abundance distributions only maintains a good representation of the vegetation in the grid cell if the majority class is present at very high majority abundance; this is the reason why we eliminated grid cells with less than 85% dominance in training the Landsat classifier. However, if the diversity within a 900m^2 grid cell is high, the dominant class can have a very low majority percentage. For example, if a grid cell has a diversity of 10 classes and most of them are equally represented, in the worst case scenario the dominant class could have just a little more than 10% dominance, yet this class would be assigned to the grid cell. The dominance percentage density plot for WE3A provided in Figure 13 demonstrates that this mixed condition is more the rule than the exception. For each community class Figure 13 plots the density of 900m^2 grid cells assigned to that class (y-axis) against the percent the class was present in the grid cell (x-axis) (i.e., for the 900m^2 grid cell, the percent of 2x2m pixels assigned that class). This plot shows that only two classes, *Nymphaea odorata* (FLno) and bayhead shrubs (SB), have a high proportion of grid cells with dominance between 80 and 100% (i.e., where the pixels were relatively homogeneous). On the other side of the spectrum is tall *Cladium* (GTcjT) with a peak in percent dominance at about 45%; thus, these grids were classified as tall sawgrass with only about 45% tall sawgrass present in the grid cell (Figure 13). Even the more general *Cladium* class (GTcj) has a broad range of percent dominance with values greater than 90% relatively rare (Figure 13). The reason why pure *Cladium* cells are not common at the 900m^2 grid is because the ridges are often narrower than 30m and are more interspersed and perforated, e.g., with pockets of broad-leaved and shrub species. In contrast, sloughs are often wider and more homogeneous (Figure 6, 7).

At lower spatial resolutions, this mixing of vegetation classes within a grid cell is common, and the questions for vegetation classification then become what mixes of classes are frequent and what mixes are rare, and can the frequent mixes be quantified in such a manner that satellite data can be used to capture and classify them (e.g., what distinguishes two wet prairie classes with the same species composition (presence) but different relative abundances of species)? One of the future challenges is to identify, quantify and name (classify) these mixed classes in order to map accurately at the coarser spatial resolutions. A specific question that could be

addressed in the context of this study is whether ordination or clustering procedures based on composition in terms of relative abundance of plant communities assist in deriving appropriate plant community classification schemes for detection at lower spatial resolutions. That is, can the data derived from this study be used to create reproducible and common mixed-pixel classes that can be used to classify vegetation across the Everglades landscape from lower resolution but readily-available remotely sensed data, such as Landsat?

To address this question, we started working with ordination and clustering techniques that would allow for data-driven classification scheme definitions based on relative abundance of dominant species at each scale of interest. Our structural level of classification was an initial result. Detectability of those classes from lower resolution data (e.g., Landsat) was increased, and maps were more accurate and meaningful, i.e., ground units (Landsat-sized pixels in the field) represented common community mixes across the landscape. The major difficulty that arises at this point is how to evaluate comparability and stability of simulated cluster and ordination results generated from random samples at specific scales (e.g., pixel size of a sensor). In this study we have made progress in the automation of random sample and ordination at arbitrary grid sizes.   We propose that a future project needs to address the issues of cluster and ordination stability to derive scale-specific classification schemata and their class definitions. Because at this time it is not necessarily desirable or feasible to conduct a high-resolution mapping effort for the entire Everglades ecosystem (i.e., using WV2 imagery across the whole ecosystem), strategically located, representative landscape units of 8-10km^2 might provide sufficient information about heterogeneity and relative abundance frequencies of communities at high spatial resolutions to develop scale-specific classification schemes. The resulting classification schemata could then be applied to lower resolution remote sensing efforts for larger whole ecosystem mapping.

Tables

Table 1. Vegetation classification schemata, including community class, species structure and commuity structure levels. Note that species are not confined to one community structure or class; rather, context determines the higher level categories. See text for acronym definitions.

landscape morphology	community structure	community class	species structure	species abr.	species name
	SL	BLsl	BL	sl	Sagittaria lancifolia
	SL	BLpc	BL	pc	Pontederia cordata
	SL	BLtg	BL	tg	Thalia geniculata
	SL	FLna	FL	na	Nuphar advena
	SL	FLno	FL	no	Nymphaea odorata
	SL	FLnq	FL	nq	Nymphoides aquatica
Marsh Freshwater Slough (MFSL)	SL	FLuf	FL	uf	Utricularia foliosa
	SL	FLuc	FL	uc	Utricularia cornuta
	SL	FLug	FL	ug	Utricularia gibba
	SL	FLup	FL	up	Utricularia purpurea
	SL	GSee	GS	ee	Eleocharis elongata
	SL	GSec	GS	ec	Eleocharis cellulosa
	SL	GSei	GS	ei	Eleocharis interstincta
	SL	Pfl	P	fl	floating periphyton
	WP	BLbc	BL	bc	Bacopa caroliniana
	WP	BLca	BL	ca	Crinum americanum
	WP	BLsl	BL	sl	Sagittaria lancifolia
	WP	BLlr	BL	lr	Ludwigia repens
	WP	BLpc	BL	pc	Pontederia cordata
	WP	BLps	BL	ps	Polygonum setaceum
	WP	FLno	FL	no	Nymphaea odorata
	WP	FLnq	FL	nq	Nymphoides aquatica
Marsh Freshwater Wet Prairie (MFWP)	WP	GSec	GS	ec	Eleocharis cellulosa
	WP	GSee	GS	ee	Eleocharis elongata
	WP	GSei	GS	ei	Eleocharis interstincta
	WP	GSph	GS	ph	Panicum hemitomon
	WP	GSpr	GS	pr	Panicum repens
	WP	GSrt	GS	rt	Rhynchospora tracyi
	WP	GSri	GS	ri	Rhynchospora inundata
	GT	GTcj	GT	cj	Cladium jamaicense
	GT	GTtd	GT	td	Typha domingensis
	WP	Pb	P	b	benthic periphyton
	S	Ssc	S	sc	Salix caroliniana
	S	Smc	S	mc	Myrica cerrifera
Marsh/Swamp Shrubland (MS or SS)	S	Sci	S	ci	Chrysobalanus icaco
	S	Sco	S	co	Cephalanthus occidentalis
	S	Slo	S	lo	Ludwigia octovalvis
	S	Slp	S	lp	Ludwigia peruviana
	T	Tag	T	ag	Annona glabra
	T	Tpb	T	pb	Persea borbonia
Swamp Forest (SF)	T	Tpp	T	pp	Persea palustris
	T	Tmv	T	mv	Magnolia virginiana
	T	Tf	T	f	Ficus
Swamp Woodland (SW)	T	Tmq	T	mq	Melaleuca quinquenervia

Table 2. Subset of community classes from Table 1 used in mapping TTB and WE3A. These classes were encountered frequently enough to classify from satellite data. TTB = N and S of the Tamiami Trail Bridge; WE3A = Western Water Conservation Area 3A.

community structure	community class	community class description	TTB	WE3A
SL	Flno	*Nymphaea odorata*	0	1
SL	FLu	*Utricularia ssp.*	0	1
SL	_Pf	floating periphyton mat	0	1
SL	_OW	open water in Slough matrix	0	1
BL	BLmix	Broadleaf mix (i.e., *Sagittaria, Pontederia, Crinum, Peltandra*)	1	1
BL	BLpv	*Peltandra virginica*	1	1
BL	BLbs	*Blechnum serrulatum*	1	1
WP	GS_BL	short graminoid broadleaf mix	1	0
WP	GSmix	short graminoid mix (i.e., *Eleocharis, Panicum, Rynchospora*)	1	0
WP	Gse	*Eleocharis ssp.*	1	0
WP	GSrt	*Rhynchospora tracyi*	1	0
WP	_Pb	benthic periphyton mat	1	0
WP	_BGp	bare ground peat (w/wo water)	1	0
GT	GTcj	*Cladium jamaicense*	1	1
GT	GTcjS	*Cladium jamaicense* Short	1	0
GT	GTcjT	*Cladium jamaicense* Tall	1	1
GT	GTt	*Typha ssp.*	1	1
S	Ssc	*Salix caroliniana*	1	1
S	SB	Bayhead (i.e., *Annona, Myrica, Persea, Magnolia*)	1	1
T	TB	Bayhead (i.e., *Annona, Myrica, Persea, Magnolia*)	1	1
T	Tag	*Annona glabra*	1	0
		total number of classes	17	13

Table 3. Spectral and spatial characteristics of the 8 reflective WorldView 2 bands (Updike and Comp 2010).

band name	center (μm)	50% band pass (μm)	5% band pass (μm)	spatial resolution (m)
(1) coastal	0.427	0.401 - 0.453	0.396 - 0.458	2
(2) blue	0.478	0.448 - 0.508	0.442 - 0.515	2
(3) green	0.546	0.511 - 0.581	0.506 - 0.586	2
(4) yellow	0.608	0.589 - 0.627	0.584 - 0.632	2
(5) red	0.659	0.629 - 0.689	0.624 - 0.694	2
(6) red edge	0.724	0.704 - 0.744	0.699 - 0.749	2
(7) near-infrared 1	0.831	0.772 - 0.89	0.765 - 0.901	2
(8) near-infrared 2	0.908	0.862 - 0.954	0.856 - 1.043	2

Table 4. Bandwidth and spatial resolution for Landsat TM and ETM+ 6 reflective bands.

band name	TM 50% band pass (μm)	ETM+ 50% band pass (μm)	spatial resolution (m)
(1) blue	0.45 - 0.52	0.45 - 0.515	30
(2) green	0.52 - 0.60	0.525 - 0.605	30
(3) red	0.63 - 0.69	0.63 - 0.69	30
(4) near-infrared	0.76 - 0.9	0.76 - 0.9	30
(5) mid-infrared 1	1.55 – 1.75	1.55 – 1.75	30
(7) mid-infrared 2	2.08 – 2.35	2.08 – 2.35	30

Table 5. Models compared for atmospheric correction of WorldView2 images. Evaluated models varied in the selection of atmospheric and aerosol models, as well as visibility parameters used.

model name	acquisition date	atmospheric model	aerosol model	visibility (Km)
Wet_MLS_vis100_Tropo	11/6/2010	Mid-latitude Summer	Tropospheric	100
Wet_MLS_vis80_Tropo	11/6/2010	Mid-latitude Summer	Tropospheric	80
Wet_MLS_vis60_Tropo	11/6/2010	Mid-latitude Summer	Tropospheric	60
Wet_MLS_vis40_Tropo	11/6/2010	Mid-latitude Summer	Tropospheric	40
Wet_MLS_vis100_Mari	11/6/2010	Mid-latitude Summer	Maritime	100
Wet_MLS_vis80_Mari	11/6/2010	Mid-latitude Summer	Maritime	80
Wet_MLS_vis60_Mari	11/6/2010	Mid-latitude Summer	Maritime	60
Wet_MLS_vis40_Mari	11/6/2010	Mid-latitude Summer	Maritime	40
Dry_MLS_vis100_Tropo	5/1/2011	Mid-latitude Summer	Tropospheric	100
Dry_MLS_vis80_Tropo	5/1/2011	Mid-latitude Summer	Tropospheric	80
Dry_MLS_vis60_Tropo	5/1/2011	Mid-latitude Summer	Tropospheric	60
Dry_MLS_vis40_Tropo	5/1/2011	Mid-latitude Summer	Tropospheric	40
Dry_MLS_vis100_Mari	5/1/2011	Mid-latitude Summer	Maritime	100
Dry_MLS_vis80_Mari	5/1/2011	Mid-latitude Summer	Maritime	80
Dry_MLS_vis60_Mari	5/1/2011	Mid-latitude Summer	Maritime	60
Dry_MLS_vis40_Mari	5/1/2011	Mid-latitude Summer	Maritime	40
Dry_TRP_vis100_Tropo	5/1/2011	Tropical	Tropospheric	100
Dry_TRP_vis80_Tropo	5/1/2011	Tropical	Tropospheric	80
Dry_TRP_vis60_Tropo	5/1/2011	Tropical	Tropospheric	60
Dry_TRP_vis40_Tropo	5/1/2011	Tropical	Tropospheric	40
Dry_TRP_vis100_Mari	5/1/2011	Tropical	Maritime	100
Dry_TRP_vis80_Mari	5/1/2011	Tropical	Maritime	80
Dry_TRP_vis60_Mari	5/1/2011	Tropical	Maritime	60
Dry_TRP_vis40_Mari	5/1/2011	Tropical	Maritime	40

Table 6. Models compared for atmospheric correction of Landsat 7 ETM+ and Landsat 5 images. Evaluated models varied in the selection of atmospheric and aerosol models, as well as visibility parameters used.

model name	satellite	sensor	acquisition date	atmospheric model	aerosol model	visibility (Km)
Wet_MLS_vis100_Rur	Landsat 5	TM	12/25/2010	Mid-latitude Summer	Rural	100
Wet _MLS_vis100_Mari	Landsat 5	TM	12/25/2010	Mid-latitude Summer	Maritime	100
Wet _TRP_vis100_Rur	Landsat 5	TM	12/25/2010	Tropical	Rural	100
Wet _TRP_vis100_Mari	Landsat 5	TM	12/25/2010	Tropical	Maritime	100
Wet _MLS_vis80_Rur	Landsat 5	TM	12/25/2010	Mid-latitude Summer	Rural	80
Wet _TRP_vis80_Rur	Landsat 5	TM	12/25/2010	Tropical	Rural	80
Wet _MLS_vis60_Rur	Landsat 5	TM	12/25/2010	Mid-latitude Summer	Rural	60
DryI_MLS_vis100_Rur	Landsat 7	ETM+	3/7/2011	Mid-latitude Summer	Rural	100
DryII _MLS_vis100_Rur	Landsat 7	ETM+	3/23/2011	Mid-latitude Summer	Rural	100
DryI_TRP_vis100_Rur	Landsat 7	ETM+	3/7/2011	Tropical	Rural	100
DryII_TRP_vis100_Rur	Landsat 7	ETM+	3/23/2011	Tropical	Rural	100
DryI_MLS_vis60_Rur	Landsat 7	ETM+	3/7/2011	Mid-latitude Summer	Rural	60
DryII_MLS_vis60_Rur	Landsat 7	ETM+	3/23/2011	Mid-latitude Summer	Rural	60

Table 7. Models from Table 5 for which the total number of pixels that lie within +/- 1% difference in reflectance after the atmospherically corrected dry season images were subtracted from atmospherically corrected wet season reference images.

reference image	compared image	pixels within +/-1% difference
Wet_MLS_vis100_Tropo	Dry_MLS_vis40_Tropo	37969
Wet_MLS_vis100_Tropo	Dry_TRP_vis40_Tropo	36308
Wet_MLS_vis100_Mari	Dry_MLS_vis40_Tropo	32564
Wet_MLS_vis80_Mari	Dry_MLS_vis40_Tropo	32419
Wet_MLS_vis80_Mari	Dry_TRP_vis40_Mari	26730
Wet_MLS_vis100_Mari	Dry_MLS_vis40_Mari	21399
Wet_MLS_Vis100_Tropo	Dry_MLS_vis40_Mari	14730
Wet_MLS_vis100_Tropo	Dry_TRP_vis40_Mari	13802
Wet_MLS_vis100_Mari	Dry_TRP_vis40_Mari	624

Table 8. List of WV2 vegetation classifier models evaluated in both TTB and WE3A areas.

prediction level	model name	variable set	classifier
community class (comClass)	wetSeason	8 refl. bands of 11/2010	randomForest (rndFor)
	drySeason	8 refl. bands of 5/2011	
	biSeason	16 refl. bands of 2010/2011	
community structure (comStruc)	wetTexture	8 refl. bands and 16 text. layers of 11/2010	Ctree (cTree)
	dryTexture	8 refl. bands and 16 text. layers of 5/2011	
	biTexture	16 refl. bands and 32 text. Layers of 2010/2011	

Table 9. Stratified random samples per class and ROI that were ground referenced (ground) and visually interpreted (total) in design-based model evaluation. TTB = N and S of the Tamiami Trail Bridge; WE3A = Western Water Conservation Area 3A; community class and structure level abbreviations from Table 2.

community structure	community class	community class description	TTB total	ground	WE3A total	ground
SL	Flno	*Nymphaea odorata*	-	-	54	10
SL	FLu	*Utricularia ssp.*	-	-	54	0
SL	_Pf	floating periphyton mat	-	-	54	4
SL	_OW	open water in Slough matrix	-	-	54	0
BL	BLmix	Broadleaf mix (i.e., *Sagittaria, Pontederia, Crinum, Peltandra*)	39	7	54	5
BL	BLpv	*Peltandra virginica*	-	-	54	0
BL	BLbs	*Blechnum serrulatum*	39	1	54	0
WP	GS_BL	short graminoid broadleaf mix	39	0	-	-
WP	GSmix	short graminoid mix (i.e., *Eleocharis, Panicum, Rynchospora*)	39	14	-	-
WP	Gse	*Eleocharis ssp.*	39	1	-	-
WP	GSrt	*Rhynchospora tracyi*	39	8	-	-
WP	_Pb	benthic periphyton mat	39	10	-	-
WP	_BGp	bare ground peat (w/wo water)	39	1	-	-
GT	GTcj	*Cladium jamaicense*	39	3	54	7
GT	GTcjS	*Cladium jamaicense* Short	39	3	-	-
GT	GTcjT	*Cladium jamaicense* Tall	39	0	54	4
GT	GTt	*Typha ssp.*	39	5	54	2
S	Ssc	*Salix caroliniana*	39	1	54	2
S	SB	Bayhead (i.e., *Annona, Myrica, Persea, Magnolia*)	39	2	54	1
T	TB	Bayhead (i.e., *Annona, Myrica, Persea, Magnolia*)	39	0	54	0
T	Tag	*Annona glabra*	39	0	-	-
		total number of samples (ground referenced)	624	56	702	35

Table 10. Summary of vegetation classification results given as percent accuracy; variable sets as described in Table 8. Data for individual models is given in the upper part of the table; means for models from different classifiers and aggregation methods are given in bold in the lower part of the table. Values for design-based overall accuracy (oaDes) and Kappa values (kaDes) are highlighted in blue. TTB = N and S of the Tamiami Trail Bridge; WE3A = Western Water Conservation Area 3A; wv2 = WorldView 2 data; ls = Landsat data; cTree = ctree classifier; rndFor = randomForest classifier; comClass = community class level of classification hierarchy; comStruc = community structure level of classification hierarchy; oaMod = model-based overall accuracy; kaMod = model-based kappa estimate; oaDes = design-based overall accuracy; kaDes = design- based kappa estimate; classAggStruc = community classes aggregated to community structure level of hierarchy.

roi	img	clf	predLevel	oaMod	kaMod	oaDes	kaDes	wet	dry	bi	wetTxt	dryTxt	biTxt
			models			accuracy				model based overall accuracy by variable set			
WE3A	wv2	cTree	comClass	87.68	84.76	-	-	81.27	63.64	84.10	84.91	69.55	87.68
WE3A	wv2	cTree	comStruc	94.61	90.81	-	-	90.96	85.24	93.16	91.60	89.34	94.61
WE3A	wv2	rndFor	comClass	90.87	88.69	-	-	81.36	64.67	86.99	86.66	73.10	90.87
WE3A	wv2	rndFor	comStruc	96.05	93.30	88.89	85.56	91.27	86.81	94.04	93.77	90.51	96.05
WE3A	wv2	rndFor	classAggStruc	96.51	94.09	-	-	-	-	-	-	-	-
WE3A	ls	rndFor	comClass	93.07	91.22	73.56	61.06	90.10	79.46	93.07	-	-	-
WE3A	ls	rndFor	classAggStruc	96.29	94.70	85.13	73.48	-	-	-	-	-	-
TTB	wv2	cTree	comClass	79.70	77.13	-	-	68.43	65.36	76.63	73.42	72.38	79.70
TTB	wv2	cTree	comStruc	91.33	86.72	-	-	85.36	84.49	89.41	88.47	85.43	91.33
TTB	wv2	rndFor	comClass	85.77	85.65	-	-	72.68	66.95	81.52	79.63	74.10	85.77
TTB	wv2	rndFor	comStruc	94.10	90.86	91.99	89.34	85.97	85.60	91.70	90.52	88.94	94.10
TTB	wv2	rndFor	classAggStruc	94.60	91.72	-	-	-	-	-	-	-	-
TTB	ls	rndFor	comClass	93.98	93.04	68.90	68.90	78.83	90.15	93.98	-	-	-
TTB	ls	rndFor	classAggStruc	98.16	97.41	82.53	62.42	-	-	-	-	-	-
			mean cTree	88.33	84.85								
			mean rndFor	91.70	89.63								
		wv2	mean Class	86.00	84.06			82.16	75.34	87.19	86.12	80.42	90.01
			mean Struc	94.02	90.42								
			mean Agg	95.55	92.90								
		ls	mean Class	93.52	92.13			84.47	84.80	93.52	-	-	-
			mean Agg	97.22	96.06								

Table 11. Model-based confusion matrix for WV2 images of TTB classified at the community class level. Community class abbreviations as in Table 2. Row abbreviations: c.T = column total; o.E(%) = omission error as a percent; acc = accuracy for column; oa = overall accuracy; K-hat = Kappa value. Column abbreviations: r.T = row total; c.E(%) = commission error as a percent.

	_BGp	_Pb	BLbs	BLmix	GS_BL	GSe	GSmix	GSrt	GTcj	GTcjS	GTcjT	GTt	SB	Ssc	Tag	TB		r.T	c.E (%)
_BGp	99	1	0	0	0	0	0	0	0	0	0	0	0	0	0	0		100	1.00
_Pb	1	146	0	0	0	0	3	1	0	2	0	0	0	0	0	0		153	4.58
BLbs	0	0	28	0	0	0	0	0	0	0	0	0	2	0	0	0		30	6.67
BLmix	0	0	0	84	0	0	0	0	2	0	2	3	0	1	0	0		92	8.70
GS_BL	0	0	0	0	127	1	4	0	0	0	0	0	0	0	0	0		132	3.79
GSe	0	1	0	0	0	57	15	4	4	5	0	1	0	0	0	0		87	34.48
GSmix	0	8	0	3	8	37	437	27	18	6	0	27	0	0	0	0		571	23.47
GSrt	0	2	0	0	0	1	4	68	0	0	0	0	0	0	0	0		75	9.33
GTcj	0	0	0	0	0	1	1	0	279	41	28	13	0	0	0	0		363	23.14
GTcjS	0	2	0	0	0	3	8	0	35	580	3	3	0	0	0	0		634	8.52
GTcjT	0	0	0	0	0	0	0	0	3	0	23	0	0	0	0	0		26	11.54
GTt	0	0	0	6	0	0	18	0	8	1	4	226	0	2	0	0		265	14.72
SB	0	0	2	0	0	0	0	0	0	0	0	0	99	0	5	7		113	12.39
Ssc	0	0	0	7	0	0	0	0	1	0	0	2	1	127	0	0		138	7.97
Tag	0	0	0	0	0	0	0	0	0	0	0	0	4	0	42	2		48	12.50
TB	0	0	0	0	0	0	0	0	0	0	0	0	14	0	3	101		118	14.41
																	2523	2945	
c.T	100	160	30	100	135	100	490	100	350	635	60	275	120	130	50	110	2945		
o.E(%)	1.00	8.75	6.67	16.00	5.93	43.00	10.82	32.00	20.29	8.66	61.67	17.82	17.50	2.31	16.00	8.18			
acc(%)	99.00	91.25	93.33	84.00	94.07	57.00	89.18	68.00	79.71	91.34	38.33	82.18	82.50	97.69	84.00	91.82			
oa(%)	85.67																		
K̂	85.65																		

Table 12. Model-based confusion matrix for WV2 images of TTB classified at the community class level then aggregated at the community structure level.   Community structure abbreviations as in Table 2. Row abbreviations: c.T = column total; o.E = omission error; o.E(%) = omission error as a percent; acc = accuracy for column; oa = overall accuracy; K-hat = Kappa value. Column abbreviations: r.T = row total; c.E = commission error; c.E(%) = commission error as a percent.

	WP	BL	GT	S	T		r.t	c.E	c.E (%)
WP	1052	3	63	0	0		1118	0.06	5.90
BL	0	112	7	3	0		122	0.08	8.20
GT	33	6	1247	2	0		1288	0.03	3.18
S	0	9	3	227	12		251	0.10	9.56
T	0	0	0	18	148		166	0.11	10.84
						2786	2945		
c.T	1085	130	1320	250	160	2945			
o.E	0.03	0.14	0.06	0.09	0.08				
o.E(%)	3.04	13.85	5.53	9.20	7.50				
acc(%)	96.96	86.15	94.47	90.80	92.50				
oa(%)	94.60								
K̂	91.72								

Table 13. Model-based confusion matrix for WV2 images of TTB classified at the community structure level. Community structure abbreviations as in Table 2. Column and row abbreviations as in Table 12.

	WP	BL	GT	S	T		r.t	c.E	c.E (%)
WP	1034	3	57	0	0		1094	0.05	5.48
BL	0	105	5	4	0		114	0.08	7.89
GT	51	10	1257	3	0		1321	0.05	4.84
S	0	12	1	220	6		239	0.08	7.95
T	0	0	0	23	154		177	0.13	12.99
						2770	2945		
c.T	1085	130	1320	250	160	2945			
o.E	0.05	0.19	0.05	0.12	0.04				
o.E(%)	4.70	19.23	4.77	12.00	3.75				
acc(%)	95.30	80.77	95.23	88.00	96.25				
oa(%)	94.06								
K̂	90.86								

Table 14. Model-based confusion matrix for Landsat images of TTB classified at the community class level. Community class abbreviations as in Table 2. Column and row abbreviations as in Table 12.

	_BGp	_Pb	BLmix	GS_BL	GSmix	GSrt	GTcj	GTcjS	GTt	SB	Ssc	Tag	r.T	c.E (%)
_BGp	19	0	0	0	0	0	0	0	0	0	0	0	19	0.00
_Pb	0	49	0	1	2	1	0	0	0	0	0	0	53	7.55
BLmix	0	0	28	0	0	0	0	0	2	1	1	0	32	12.50
GS_BL	0	0	0	1	0	0	0	0	0	0	0	0	1	100.00
GSmix	0	1	0	0	44	3	0	2	0	0	0	0	50	12.00
GSrt	0	0	0	0	0	0	0	0	0	0	0	0	0	-
GTcj	1	0	1	1	0	0	98	3	0	0	0	0	104	5.77
GTcjS	0	0	0	0	4	1	1	95	0	0	0	0	101	5.94
GTt	0	0	0	0	0	0	1	0	17	0	0	0	18	5.56
SB	0	0	0	0	0	0	0	0	0	46	0	1	47	2.13
Ssc	0	0	1	0	0	0	0	0	1	3	99	0	104	4.81
Tag	0	0	0	0	0	0	0	0	0	0	0	19	19	0.00
													515	548
c.T	20	50	30	3	50	5	100	100	20	50	100	20	548	
o.E(%)	5.00	2.00	6.67	66.67	12.00	100.00	2.00	5.00	15.00	8.00	1.00	5.00		
acc(%)	95.00	98.00	93.33	33.33	88.00	0.00	98.00	95.00	85.00	92.00	99.00	95.00		
oa(%)	93.98													
K̂	93.04													

Table 15. Model-based confusion matrix for Landsat images of TTB classified at the community class level then aggregated at the structure level. Community structure abbreviations as in Table 2. Column and row abbreviations as in Table 12.

	WP	BL	GT	S	T		r.t	c.E	c.E (%)
WP	177	0	2	0	0		179	0.01	1.12
BL	0	28	2	2	0		32	0.13	12.50
GT	1	1	215	0	0		217	0.01	0.92
S	0	1	1	148	1		151	0.02	1.99
T	0	0	0	0	19		19	0.00	0.00
						587	598		
c.T	178	30	220	150	20	598			
o.E	0.01	0.07	0.02	0.01	0.05				
o.E(%)	0.56	6.67	2.27	1.33	5.00				
acc(%)	99.44	93.33	97.73	98.67	95.00				
oa(%)	98.16								
$\hat{K}$	97.41								

Table 16. Model-based confusion matrix for WV2 images of WE3A classified at the community class level. Community class abbreviations as in Table 2. Column and row abbreviations as in Table 12.

	_OW	_Pf	BLbs	BLmix	BLpv	FLno	FLu	GTcj	GTcjT	GTt	SB	Ssc	TB		r.T	c.E	c.E (%)
_OW	95	0	0	0	0	6	0	0	0	0	0	0	0		101	0.06	5.94
_Pf	0	578	0	3	0	44	12	0	0	1	0	0	0		638	0.09	9.40
BLbs	0	0	44	4	0	0	0	0	0	0	6	0	2		56	0.21	21.43
BLmix	1	0	0	197	7	4	0	7	0	0	0	0	2		218	0.10	9.63
BLpv	0	0	1	3	51	1	0	1	0	0	0	2	0		59	0.14	13.56
FLno	4	50	0	21	9	1060	0	6	1	0	0	0	0		1151	0.08	7.91
FLu	0	2	0	0	0	0	68	0	0	0	0	0	0		70	0.03	2.86
GTcj	0	0	0	9	7	5	0	520	24	11	0	3	0		579	0.10	10.19
GTcjT	0	0	0	0	1	0	0	7	70	2	0	0	0		80	0.13	12.50
GTt	0	0	0	0	0	0	0	8	0	82	0	1	0		91	0.10	9.89
SB	0	0	3	0	0	0	0	0	5	0	67	2	3		80	0.16	16.25
Ssc	0	0	1	3	0	0	0	1	0	4	0	92	0		101	0.09	8.91
TB	0	0	1	0	0	0	0	0	0	0	2	0	93		96	0.03	3.13
														3017	3320		
c.T	100	630	50	240	75	1120	80	550	100	100	75	100	100	3320			
o.E	0.05	0.08	0.12	0.18	0.32	0.05	0.15	0.05	0.30	0.18	0.11	0.08	0.07				
o.E(%)	5.00	8.25	12.00	17.92	32.00	5.36	15.00	5.45	30.00	18.00	10.67	8.00	7.00				
acc(%)	95.00	91.75	88.00	82.08	68.00	94.64	85.00	94.55	70.00	82.00	89.33	92.00	93.00				
oa(%)	90.87																
$\hat{K}$	88.69																

Table 17. Model-based confusion matrix for WV2 imagery of WE3A classified at the community class level then aggregated at the community structure level. Community structure abbreviations as in Table 2. Column and row abbreviations as in Table 12.

	SL	BL	GT	S	T		r.t	c.E	c.E (%)
SL	1919	33	8	0	0		1960	0.02	2.09
BL	6	307	8	8	4		333	0.08	7.81
GT	5	17	724	4	0		750	0.03	3.47
S	0	7	10	161	3		181	0.11	11.05
T	0	1	0	2	93		96	0.03	3.13
						3204	3320		
c.T	1930	365	750	175	100	3320			
o.E	0.01	0.16	0.03	0.08	0.07				
o.E(%)	0.57	15.89	3.47	8.00	7.00				
acc(%)	99.43	84.11	96.53	92.00	93.00				
oa(%)	96.51								
$\hat{K}$	94.09								

Table 18. Model-based confusion matrix for WV2 imagery of WE3A classified at the community structure level. Community structure abbreviations as in Table 2. Column and row abbreviations as in Table 12.

	SL	BL	GT	S	T		r.t	c.E	c.E (%)
SL	1922	36	16	0	0		1974	0.03	2.63
BL	4	300	8	9	4		325	0.08	7.69
GT	4	22	714	3	0		743	0.04	3.90
S	0	6	12	160	3		181	0.12	11.60
T	0	1	0	3	93		97	0.04	4.12
						3189	3320		
c.T	1930	365	750	175	100	3320			
o.E	0.00	0.18	0.05	0.09	0.07				
o.E(%)	0.41	17.81	4.80	8.57	7.00				
acc(%)	99.59	82.19	95.20	91.43	93.00				
oa(%)	96.05								
$\hat{K}$	93.30								

Table 19. Model-based confusion matrix for WE3A for Landsat classified at community class level. Community class abbreviations as in Table 2. Column and row abbreviations as in Table 12.

	_OW	_Pf	BLbs	BLmix	BLpv	FLno	GTcj	SB	Ssc	TB		r.T	c.E	c.E (%)
_OW	2	0	0	0	0	0	0	0	0	0		2	0.00	0.00
_Pf	0	42	0	0	0	1	0	0	0	0		43	0.02	2.33
BLbs	0	0	17	0	1	0	0	2	0	0		20	0.15	15.00
BLmix	0	0	0	4	0	0	2	0	0	0		6	0.33	33.33
BLpv	0	0	0	0	2	0	0	0	0	0		2	0.00	0.00
FLno	3	8	0	0	0	98	0	0	0	0		109	0.10	10.09
GTcj	0	0	0	4	0	1	98	0	1	0		104	0.06	5.77
SB	0	0	2	0	0	0	0	98	0	2		102	0.04	3.92
Ssc	0	0	1	0	0	0	0	0	15	0		16	0.06	6.25
TB	0	0	0	0	0	0	0	0	0	0		0	-	-
											376	404		
c.T	5	50	20	8	3	100	100	100	16	2	404			
o.E	0.60	0.16	0.15	0.50	0.33	0.02	0.02	0.02	0.06	1.00				
o.E(%)	60.00	16.00	15.00	50.00	33.33	2.00	2.00	2.00	6.25	100.00				
acc(%)	40.00	84.00	85.00	50.00	66.67	98.00	98.00	98.00	93.75	0.00				
oa(%)	93.07													
K̂	91.22													

Table 20. Model-based confusion matrix for WE3A for Landsat classified at community class level aggregated at community structure level. Community structure abbreviations as in Table 2. Column and row abbreviations as in Table 12.

	SL	BL	GT	S	T		r.t	c.E	c.E (%)
SL	154	0	0	0	0		154	0.00	0.00
BL	0	24	2	2	0		28	0.14	14.29
GT	1	4	98	1	0		104	0.06	5.77
S	0	3	0	113	2		118	0.04	4.24
T	0	0	0	0	0		0	-	-
						389	404		
c.T	155	31	100	116	2	404			
o.E	0.01	0.23	0.02	0.03	1.00				
o.E(%)	0.65	22.58	2.00	2.59	100.00				
acc(%)	99.35	77.42	98.00	97.41	0.00				
oa(%)	96.29								
K̂	94.70								

Table 21. Design-based post-classification accuracy assessment results for TTB for ground referenced and stereo interpreted sample evaluations of community structure. Detailed sample distribution by community class as in Table 9. Community structure abbreviations as in Table 2. Column and row abbreviations as in Table 12.

	WP	BL	GT	S	T		r.t	c.E	c.E (%)
WP	221	1	11	0	0		233	0.05	5.15
BL	0	53	3	16	5		77	0.31	31.17
GT	0	0	155	2	0		157	0.01	1.27
S	0	0	0	79	0		79	0.00	0.00
T	0	0	4	8	66		78	0.15	15.38
						574	624		
c.T	221	54	173	105	71	624			
o.E	0.00	0.02	0.10	0.25	0.07				
o.E(%)	0.00	1.85	10.40	24.76	7.04				
acc(%)	100.00	98.15	89.60	75.24	92.96				
oa(%)	91.99								
K̂	89.34								

Table 22. Design-based post-classification accuracy assessment results for WE3A for ground referenced and stereo interpreted sample evaluations of community structure. Detailed sample distribution by community class as in Table 9. Community structure abbreviations as in Table 2. Column and row abbreviations as in Table 12.

	SL	BL	GT	S	T		r.t	c.E	c.E (%)
SL	213	2	1	0	0		216	0.01	1.39
BL	1	133	19	8	1		162	0.18	17.90
GT	0	3	155	3	0		161	0.04	3.73
S	0	21	5	70	13		109	0.36	35.78
T	0	0	0	1	53		54	0.02	1.85
						624	702		
c.T	214	159	180	82	67	702			
o.E	0.00	0.16	0.14	0.15	0.21				
o.E(%)	0.47	16.35	13.89	14.63	20.90				
acc(%)	99.53	83.65	86.11	85.37	79.10				
oa(%)	88.89								
K̂	85.56								

Table 23. Results of morphological (mmu) and grid (grd)-based pixel aggregation for the area north of the Tamiami Trail Bridge (NOTA), given as percent of community class (comClass) or community structural class (comStruc) present in the mapped region of interest. Community class and community structural class abbreviations as in Table 2. Column colors indicate the following: light blue = classified from WorldView 2 (wv2) or Landsat (ls) satellite data; white = wv2 aggregated by 5 ($20m^2$), 10 ($40m^2$), and 100 ($400m^2$) pixels; orange = wv2 aggregated at Landsat resolution ($900m^2$); green = wv2 aggregated at CERP grid resolution ($2500m^2$). Aggregation method "mmu" indicates morphological aggregation, "grd" indicates grid-based aggregation; numbers following these abbreviations are the square meters in the minimum mapping unit or grid.

comClass	wv2	mmu20	mmu40	mmu400	mmu900	grd900	ls	mmu2500	grd2500
_BGp	3.2	3.1	3.0	2.3	1.9	2.2	4.3	1.3	1.5
_OW	0.0	0.0	0.0	-	-	0.0	-	-	-
_Pb	4.8	4.8	4.8	4.8	4.8	5.1	5.0	4.9	5.5
BLbs	0.1	0.1	0.1	0.1	0.1	0.0	-	0.1	-
BLmix	3.6	3.5	3.4	3.1	2.9	3.6	5.9	2.6	3.2
GS_BL	1.2	1.2	1.2	1.1	1.1	1.0	0.7	1.1	0.6
GSe	1.1	1.1	1.1	1.1	1.1	0.1	-	1.0	0.0
GSmix	11.1	10.9	10.8	10.1	9.7	10.3	8.9	9.1	8.7
GSrt	3.0	3.0	3.0	3.0	2.9	1.5	1.7	2.8	1.3
GTcj	41.9	42.1	42.3	43.2	43.7	48.8	47.2	44.4	51.7
GTcjS	22.7	22.8	22.9	23.6	24.0	21.1	20.6	24.7	21.3
GTcjT	0.0	0.0	0.0	0.0	0.1	-	-	0.1	-
GTt	3.6	3.7	3.8	4.2	4.3	2.9	2.4	4.8	2.6
SB	0.4	0.4	0.4	0.4	0.4	0.4	0.2	0.4	0.4
Ssc	3.2	3.2	3.1	2.9	2.9	3.0	3.0	2.8	3.1
Tag	0.0	0.0	0.0	0.0	-	-	0.0	-	-
TB	0.1	0.1	0.0	0.0	0.0	0.0	-	-	-
total	100	100	100	100	100	100	100	100	100
diversity	17	17	17	16	15	14	12	14	12
comStruc	wv2	mmu20	mmu40	mmu400	mmu900	grd900	ls	mmu2500	grd2500
BL	3.7	3.6	3.5	3.2	3.0	3.1	5.9	2.6	2.8
GT	68.3	68.7	69.1	71.1	72.1	72.8	70.2	74.0	75.1
S	3.6	3.5	3.5	3.3	3.4	3.4	3.2	3.2	3.3
SL	0.0	0.0	0.0	-	-	0.0	-	-	-
T	0.1	0.1	0.1	0.0	0.0	0.0	0.0	-	-
WP	24.4	24.1	23.8	22.4	21.6	20.7	20.6	20.2	18.8
total	100	100	100	100	100	100	100	100	100
diversity	6	6	6	5	5	6	4	4	4

Table 24. Results of morphological (mmu) and grid (grd)-based pixel aggregation for the area south of the Tamiami Trail Bridge (SOTA), given as percent of community class (comClass) or community structural class (comStruc) present in the mapped region of interest. Community class and community structural class abbreviations as in Table 2. Column colors indicate the following: light blue = classified from WorldView 2 (wv2) or Landsat (ls) satellite data; white = wv2 aggregated by 5 ($20m^2$), 10 ($40m^2$), and 100 ($400m^2$) pixels; orange = wv2 aggregated at Landsat resolution ($900m^2$); green = wv2 aggregated at CERP grid resolution ($2500m^2$). Aggregation method "mmu" indicates morphological aggregation, "grd" indicates grid-based aggregation; numbers following these abbreviations are the square meters in the minimum mapping unit or grid.

comClass	wv2	mmu20	mmu40	mmu400	mmu900	grd900	ls	mmu2500	grd2500
_BGp	0.0	-	-	-	-	-	-	-	-
_OW	0.0	0.0	0.0	-	-	-	-	-	-
_Pb	2.1	2.1	2.1	2.0	1.9	1.4	0.6	1.7	1.1
BLbs	0.3	0.2	0.2	0.1	0.0	0.0	-	0.0	-
BLmix	3.9	3.6	3.4	2.6	2.2	3.0	7.7	1.6	2.6
GS_BL	0.0	0.0	0.0	0.0	0.0	-	-	0.0	-
GSe	2.0	1.9	1.9	1.7	1.6	0.9	-	1.3	0.6
GSmix	12.4	11.9	11.5	9.7	8.9	8.7	12.4	7.3	7.2
GSrt	0.1	0.1	0.1	0.1	0.1	0.0	-	0.1	-
GTcj	20.5	20.7	20.8	21.5	21.7	22.1	10.8	22.1	21.9
GTcjS	39.7	40.1	40.4	41.8	42.6	45.9	48.1	44.0	48.4
GTcjT	1.0	1.1	1.1	1.2	1.2	0.2	-	1.3	0.1
GTt	6.4	6.5	6.6	7.1	7.3	5.2	8.2	7.7	5.0
SB	1.7	1.8	1.8	1.9	1.9	1.9	1.8	2.0	1.9
Ssc	9.3	9.4	9.5	9.8	9.9	10.3	10.0	10.3	10.7
Tag	0.4	0.4	0.4	0.4	0.4	0.4	0.4	0.4	0.4
TB	0.2	0.2	0.2	0.1	0.1	0.1	-	0.1	0.1
total	100	100	100	100	100	100	100	100	100
diversity	17	16	16	15	15	14	9	15	12
comStruc	wv2	mmu20	mmu40	mmu400	mmu900	grd900	ls	mmu2500	grd2500
BL	4.2	3.9	3.6	2.7	2.2	2.4	7.7	1.6	1.9
GT	67.6	68.3	68.8	71.6	72.8	73.5	67.1	75.2	75.3
S	11.0	11.2	11.3	11.7	11.9	11.8	11.8	12.3	12.2
SL	0.0	0.0	0.0	-	-	-	-	-	-
T	0.6	0.6	0.6	0.6	0.6	0.5	0.4	0.5	0.5
WP	16.6	16.1	15.7	13.5	12.5	11.7	13.0	10.5	10.1
total	100	100	100	100	100	100	100	100	100
diversity	6	6	6	5	5	5	5	5	5

Table 25. Results of morphological (mmu) and grid (grd)-based pixel aggregation for western Water Conservation Area 3A (WE3A), given as percent of community class (comClass) or community structural class (comStruc) present in the mapped region of interest. Community class and community structural class abbreviations as in Table 2. Column colors indicate the following: light blue = classified from WorldView 2 (wv2) or Landsat (ls) satellite data; white = wv2 aggregated by 5 ($20m^2$), 10 ($40m^2$), and 100 ($400m^2$) pixels; orange = wv2 aggregated at Landsat resolution ($900m^2$); green = wv2 aggregated at CERP grid resolution ($2500m^2$). Aggregation method "mmu" indicates morphological aggregation, "grd" indicates grid-based aggregation; numbers following these abbreviations are the square meters in the minimum mapping unit or grid.

comClass	wv2	mmu20	mmu40	mmu400	mmu900	grd900	ls	mmu2500	grd2500
_OW	0.9	0.9	0.9	0.9	0.9	0.4	0.4	0.9	0.3
_Pf	9.4	9.4	9.4	9.6	9.7	7.2	16.7	10.0	6.0
BLbs	1.3	1.3	1.3	1.4	1.4	1.3	2.4	1.3	1.4
BLmix	3.7	3.3	3.0	1.6	1.2	1.2	5.1	0.9	0.7
BLpv	0.8	0.8	0.8	0.7	0.7	0.6	0.2	0.7	0.6
FLno	46.6	46.6	46.6	47.2	47.6	50.1	39.4	48.8	51.8
FLu	0.0	0.0	0.0	0.0	0.0	-	-	0.0	-
GTcj	31.1	31.5	31.8	32.8	32.7	34.1	32.5	31.7	34.7
GTcjT	1.0	1.0	1.0	1.0	1.0	0.2	-	1.1	0.0
GTt	0.3	0.3	0.3	0.3	0.3	0.1	-	0.3	0.0
SB	2.9	2.9	3.0	3.0	2.9	3.0	2.4	2.9	2.9
Ssc	1.5	1.5	1.5	1.2	1.1	1.3	1.1	0.9	1.1
TB	0.5	0.5	0.5	0.5	0.4	0.5	0.0	0.5	0.5
total	100	100	100	100	100	100	100	100	100
diversity	13	13	13	13	13	12	10	13	12
comStruc	**wv2**	**mmu20**	**mmu40**	**mmu400**	**mmu900**	**grd900**	**ls**	**mmu2500**	**grd2500**
BL	5.9	5.4	5.1	3.7	3.2	3.2	7.7	2.9	3.0
GT	32.3	32.7	33.0	34.0	34.0	32.7	32.5	33.0	31.7
S	4.4	4.4	4.4	4.2	4.1	4.2	3.4	3.8	3.8
SL	56.8	56.9	56.9	57.6	58.2	59.4	56.4	59.8	61.1
T	0.5	0.5	0.5	0.5	0.4	0.5	0.0	0.5	0.4
total	100	100	100	100	100	100	100	100	100
diversity	5	5	5	5	5	5	5	5	5

Figures
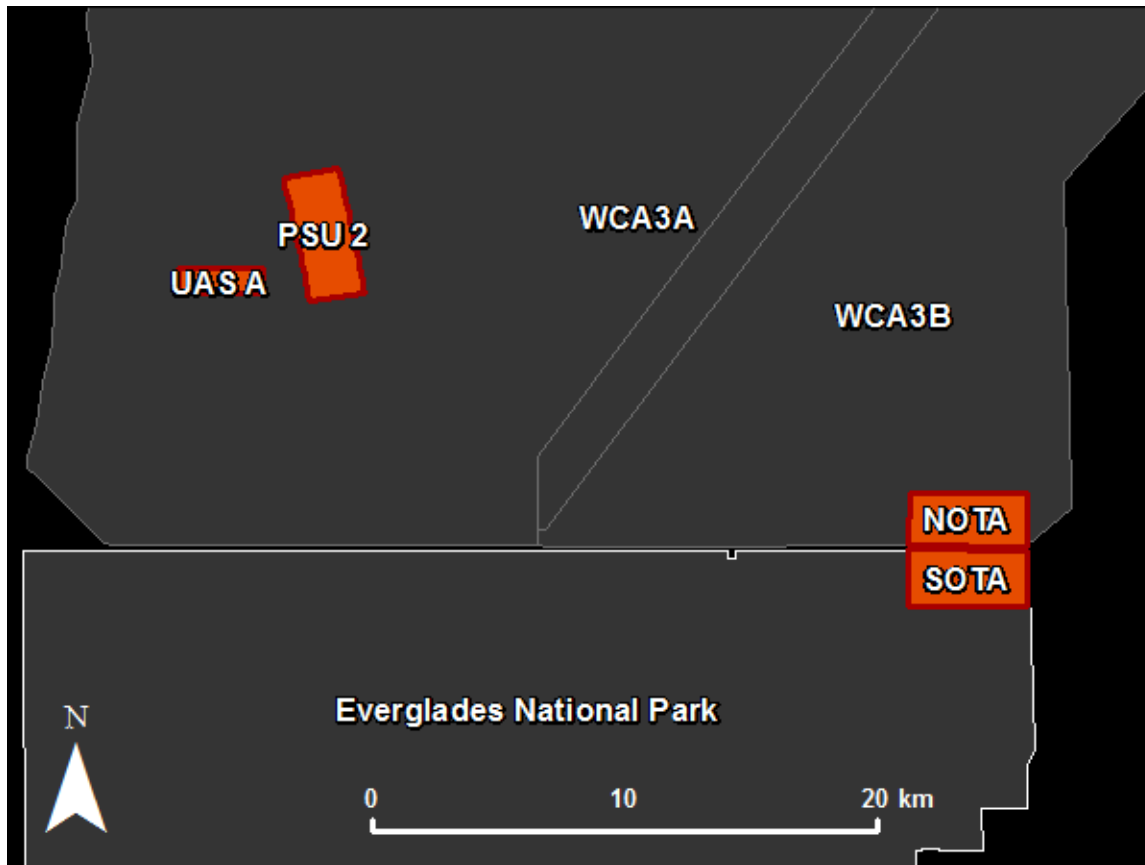
Figure 1. South Florida regions of interest (red) for which WorldView2 and Landsat data were acquired for modeling, mapping and aggregation comparisons; NOTA = NOrth of TAmiami Trail; SOTA = SOuth of TAmiami Trail, which combined are referred to as TTB = Tamiami Trail Bridge area; PSU2 = Comprehensive Everglades Restoration Plan (CERP) Primary Samplig Unit 2; UASA = Unmanned Aerial System (UAS) area A (under study by the Florida Cooperative Fish and Wildlife Research Unit's Unmanned Aerial Systems Research Group at University of Florida). PSU2 and UASA combined are referred to as WE3A = WEstern Water Conservation Area 3A.
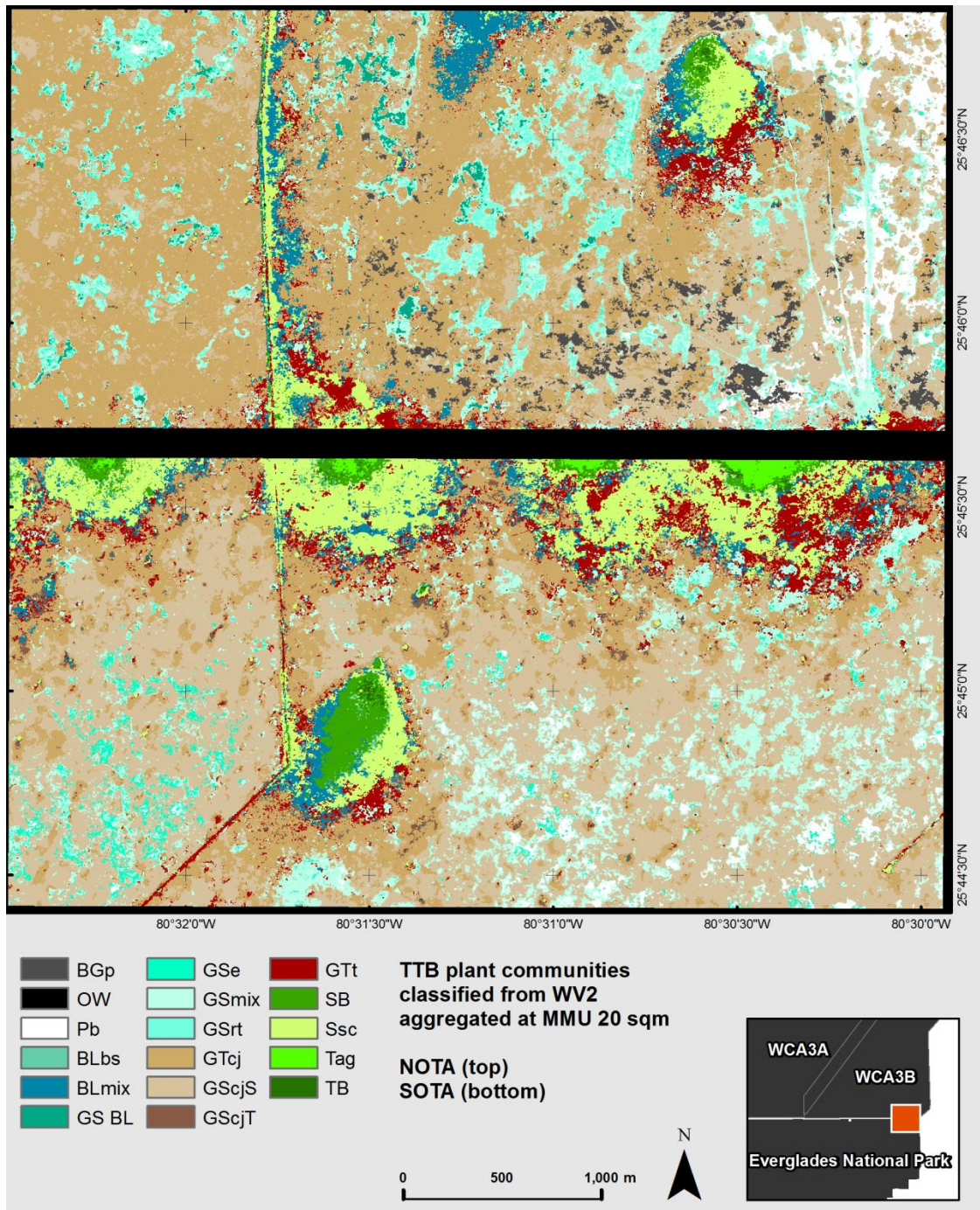
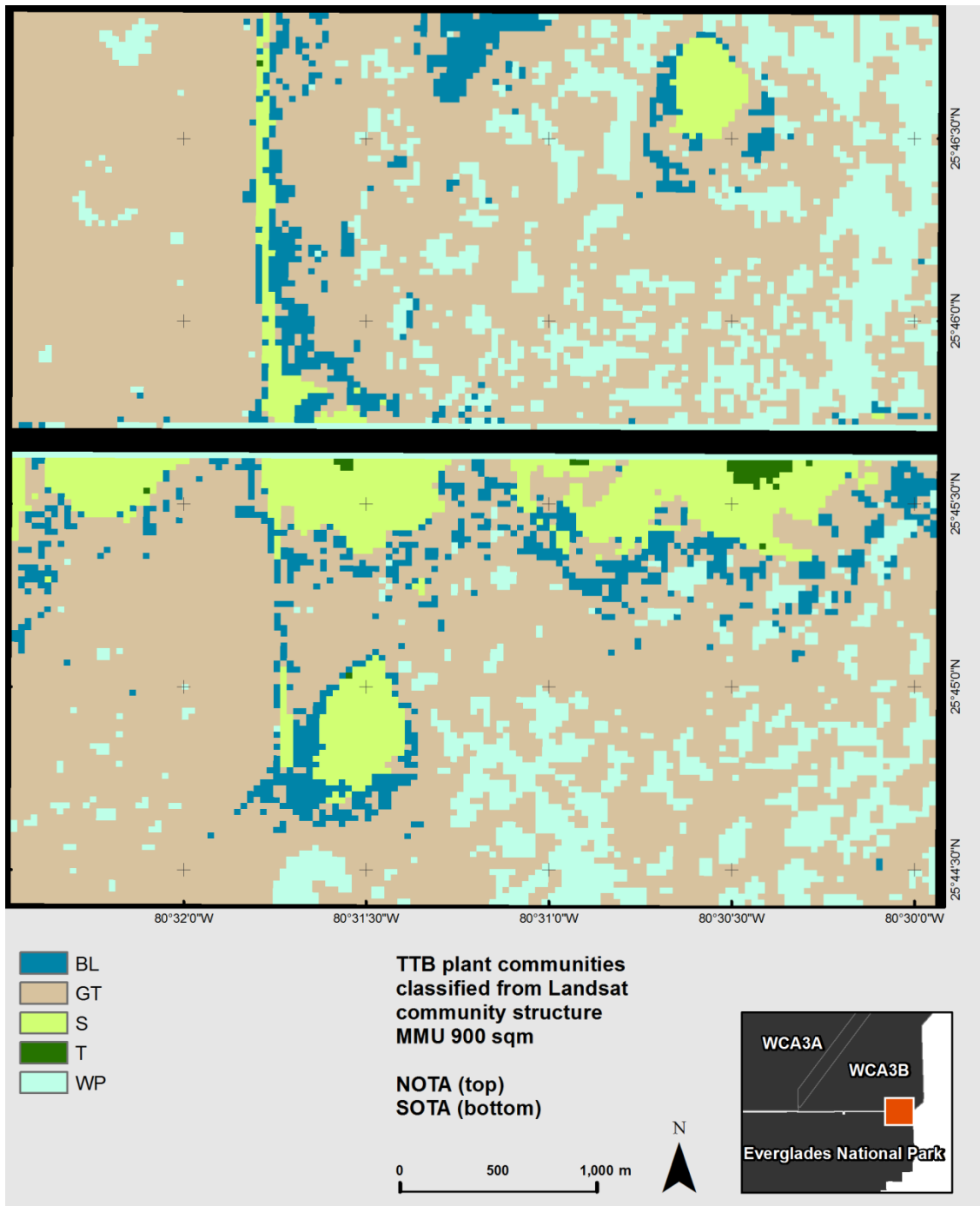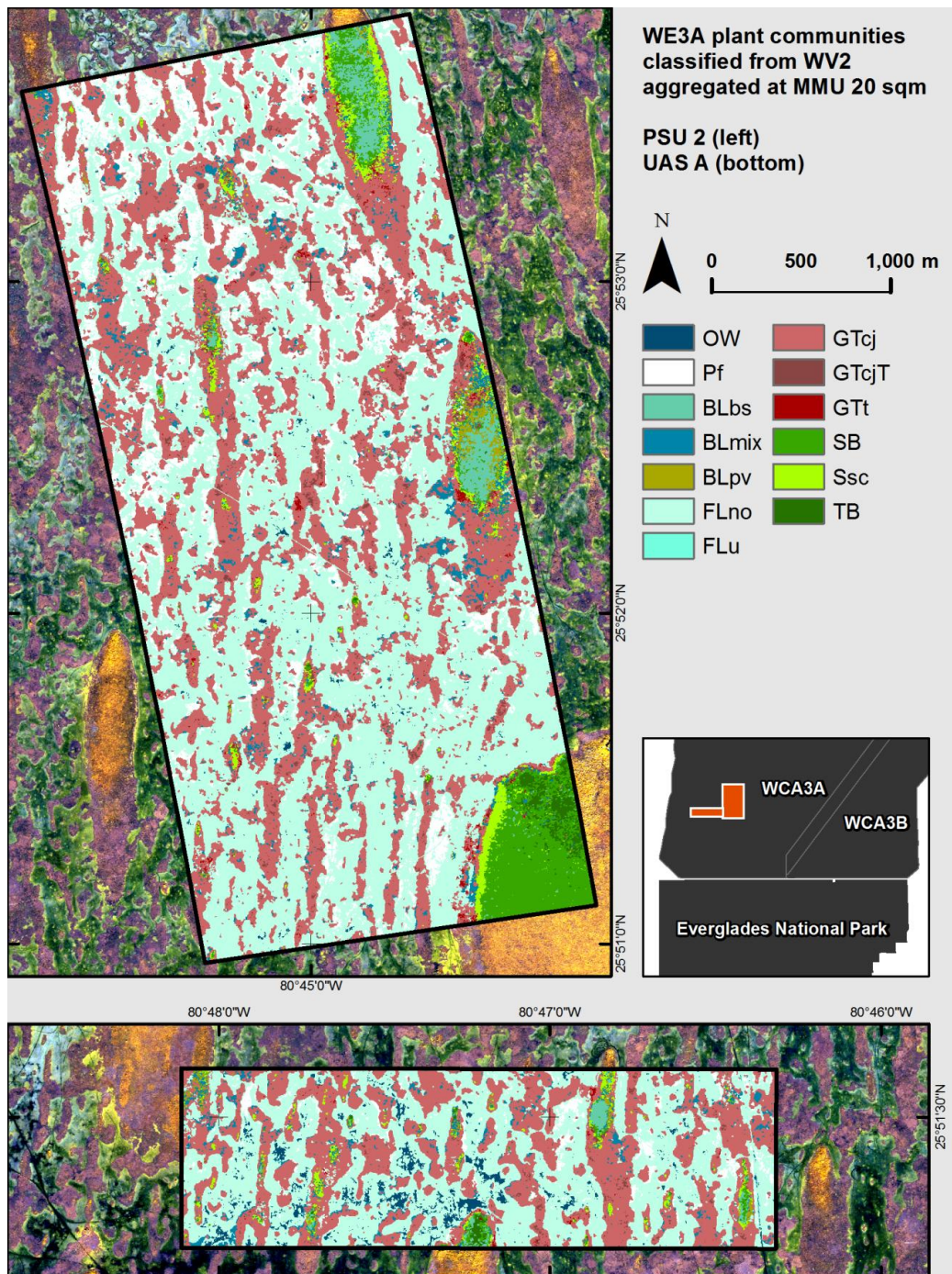**Figure 2. Vegetation classification result for TTB classified from WV2 at the community class level, aggregated at 20m² MMU. Classes: Bare Ground peat (BGp); Open Water (OW); benthic Periphyton (Pb); Broad-Leaved *Blechnum serrulatum* (BLbs); Broad-Leaved mix (BLmix); Short Graminoid Broad-Leaved mix (GS BL); Short Graminoid *Eleocharis* (GSe); Short Graminoid mix (GSmix); Short Graminoid *Rhynchospora tracyi* (GSrt); Tall Graminoid *Cladium jamaicense* (GTcj); Short (GTcjS) and Tall (GTcjT) ; Tall Graminoid *Typha* (GTt); Bayhead Shrub (SB); Shrub *Salix caroliniana* (Ssc); Tree *Annona glabra* (Tag); Bayhead Trees (TB).**
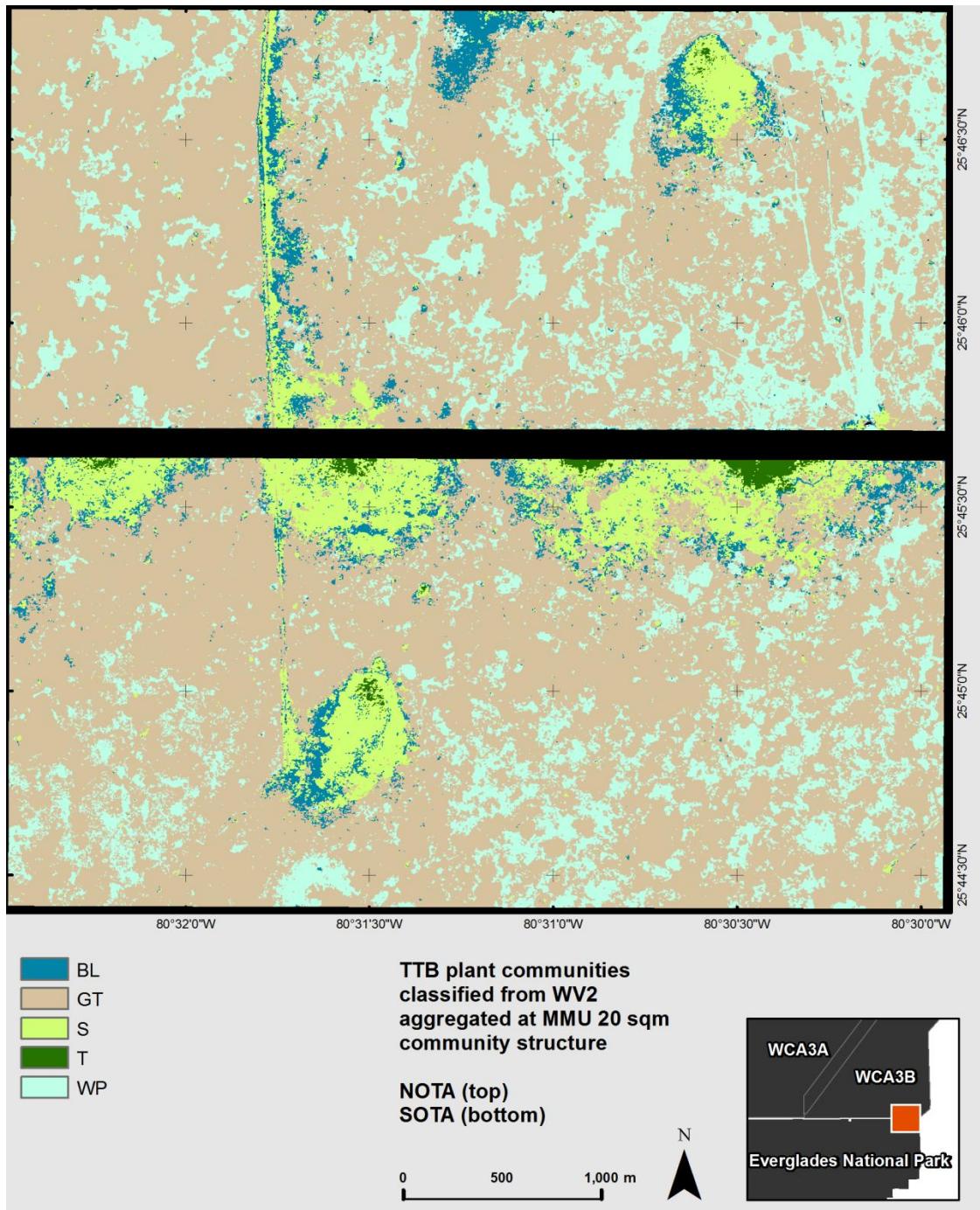
Figure 3. Vegetation classification result for TTB classified from WV2 at the community class level, aggregated at the community structure level at 20m^2 MMU. Classes: Broad-Leaved (BL); Tall Graminoid (GT); Shrub (S); Tree (T); and Wet Prairie (WP).
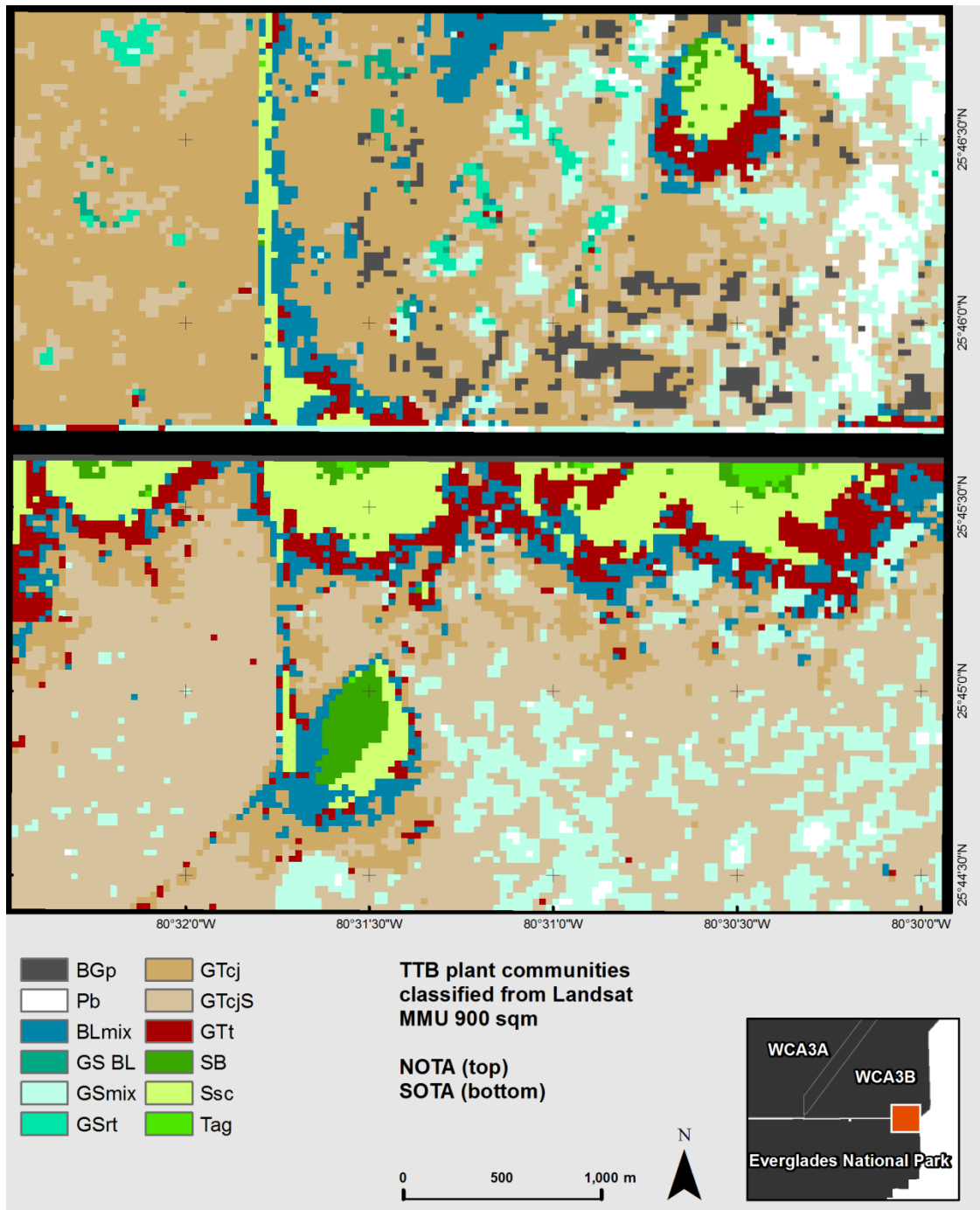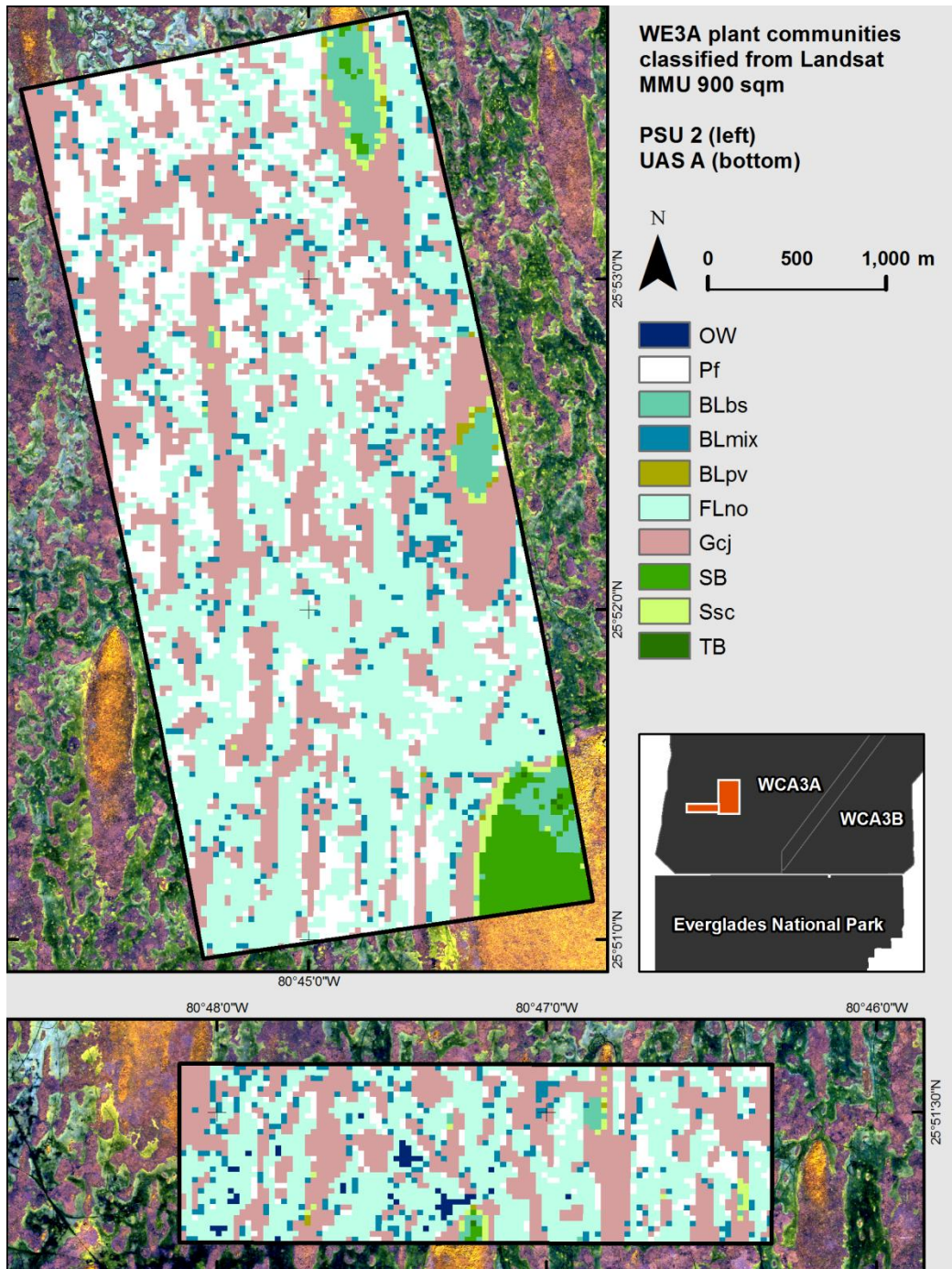
Figure 4. Vegetation classification result for TTB classified from Landsat at the community class level. Classes: Bare Ground peat (BGp); Open Water (OW); benthic Periphyton (Pb); Broad-Leaved mix (BLmix); Short Graminoid Broad-Leaved mix (GS BL); Short Graminoid mix (GSmix); Short Graminoid *Rhynchospora tracyi* (GSrt); Tall Graminoid *Cladium jamaicense* (GTcj); Short (GTcjS); Tall Graminoid *Typha* (GTt); Bayhead Shrub (SB); Shrub *Salix caroliniana* (Ssc); Tree *Annona glabra* (Tag).
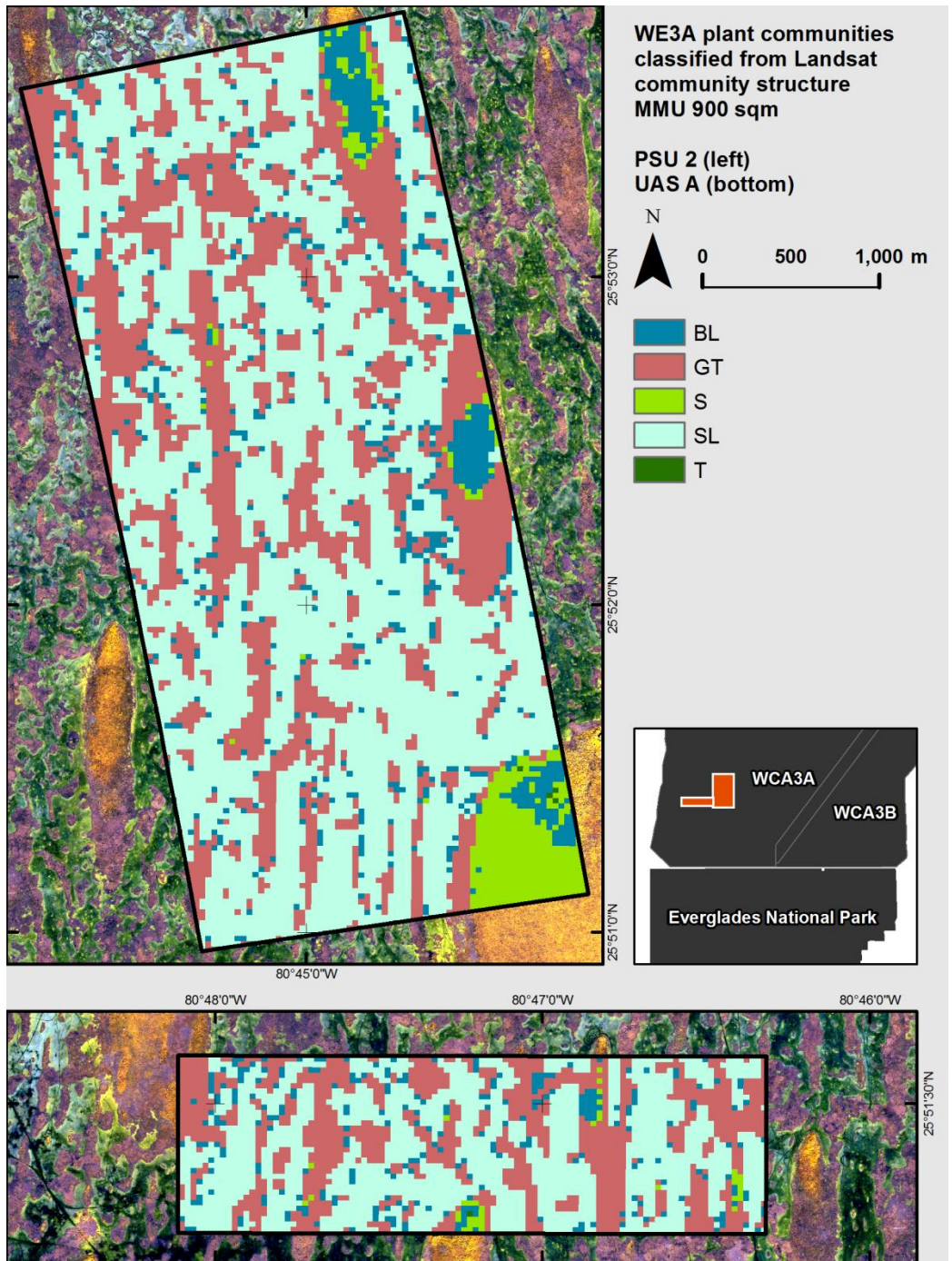
Figure 5. Vegetation classification result for TTB classified from Landsat at the community class level, aggregated at the community structure level. Classes: Broad-Leaved (BL); Tall Graminoid (GT); Shrub (S); Tree (T); and Wet Prairie (WP).

Figure 6. Vegetation classification result for WE3A classified from WV2 at the community class level, aggregated at 20m² MMU. Classes: Open Water (OW); floating Periphyton (Pf); Broad-Leaved *Blechnum serrulatum* (BLbs); Broad-Leaved mix (BLmix); Broad-Leaved *Peltandra virginica* (BLpv); Floating-Leaved *Nymphaea odorata* (FLno); Floating-Leaved *Utricularia* (FLu); Tall Graminoid *Cladium jamaicense* (GTcj); Tall (GTcjT); Tall Graminoid *Typha* (GTt); Bayhead Shrub (SB); Shrub *Salix caroliniana* (Ssc); Bayhead Tree (TB).

Figure 7. Vegetation classification result for WE3A classified from WV2 at the community class level, aggregated at the community structure level at 20m^2 MMU. Classes: Broad-Leaved (BL); Tall Graminoid (GT); Shrub (S); Slough (SL) and Tree (T).

Figure 8. Vegetation classification result for WE3A classified from Landsat at the community class level. Classes: Open Water (OW); floating Periphyton (Pf); Broad-Leaved *Blechnum serrulatum* (BLbs); Broad-Leaved mix (BLmix); Broad-Leaved *Peltandra virginica* (BLpv); Floating-Leaved *Nymphaea odorata* (FLno); Tall Graminoid *Cladium jamaicense* (GTcj); Bayhead Shrub (SB); Shrub *Salix caroliniana* (Ssc); Bayhead Tree (TB).

Figure 9. Vegetation classification result for WE3A classified from Landsat at the community class level, aggregated at the community structure level. Classes: Broad-Leaved (BL); Tall Graminoid (GT); Shrub (S); Slough (SL) and Tree (T).
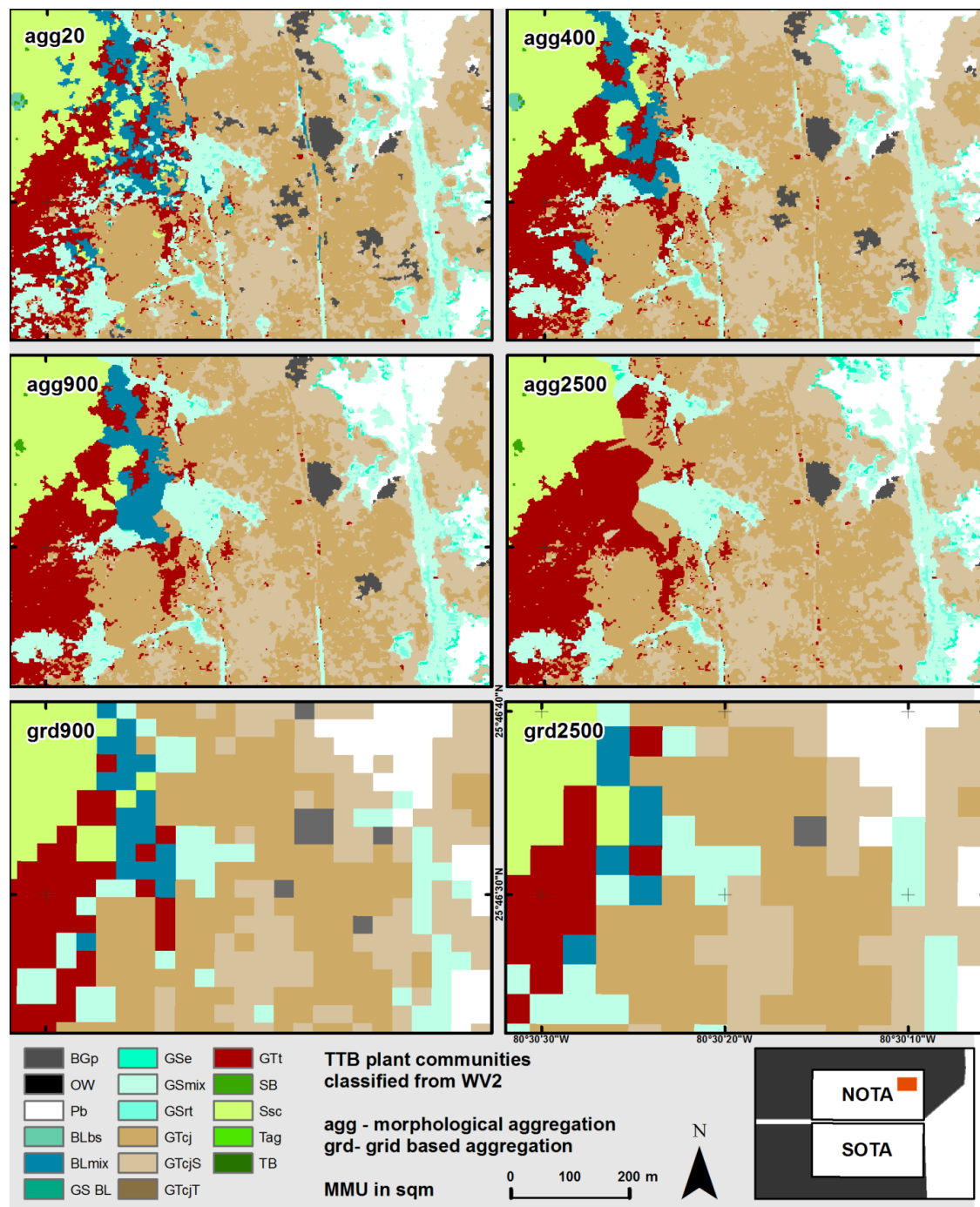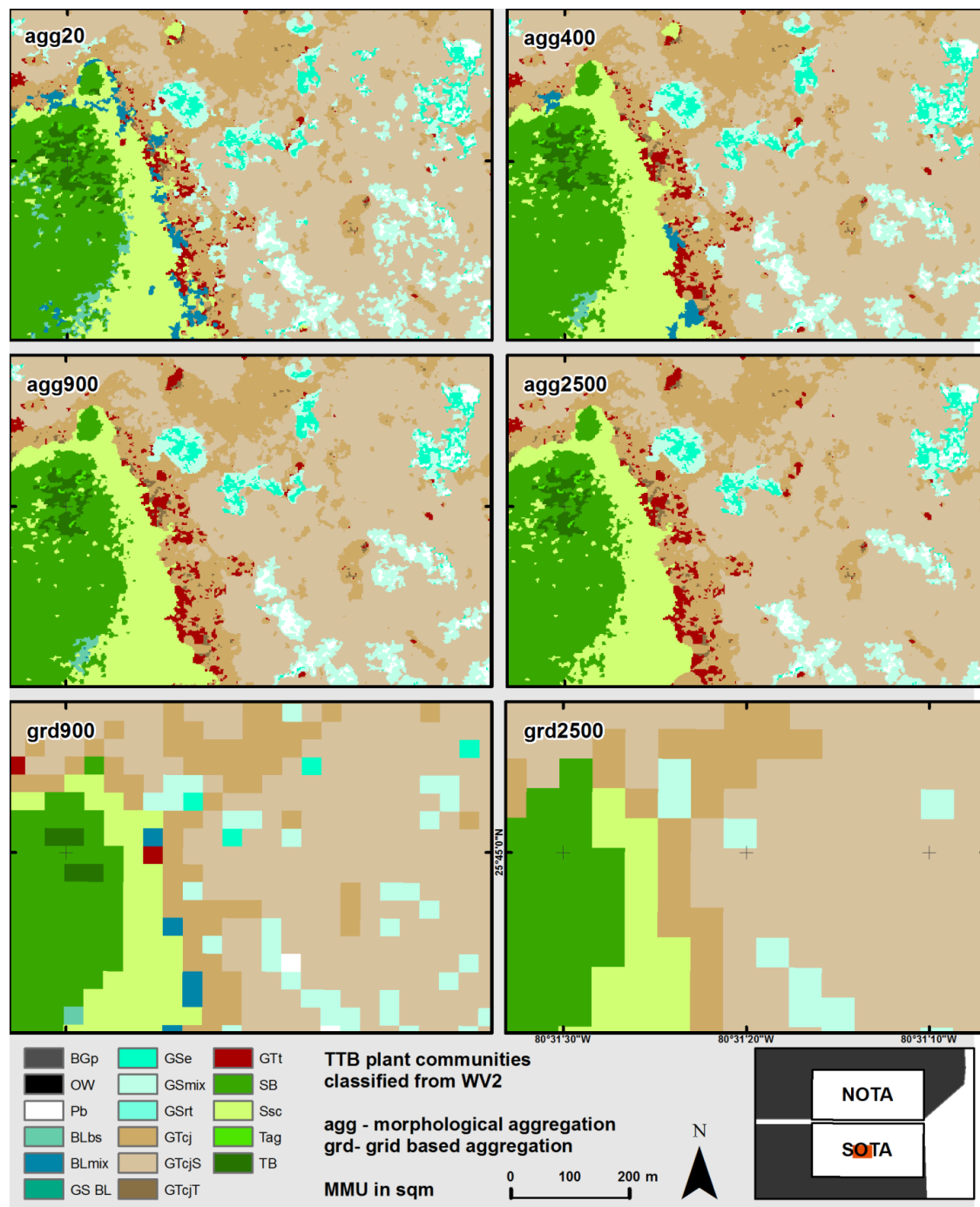
Figure 10. Comparison of morphological aggregation (agg) at 20, 400, 900 and 2500m^2 and grid-based aggregation (grd) at 900m^2 (MMU equivalent to Landsat pixels) and 2500m^2 (MMU equivalent to CERP grids) for a subset of the area north of Tamiami Trail. Classes: Bare Ground peat (BGp); Open Water (OW); benthic Periphyton (Pb); Broad-Leaved *Blechnum serrulatum* (BLbs); Broad-Leaved mix (BLmix); Short Graminoid Broad-Leaved mix (GS BL); Short Graminoid *Eleocharis* (GSe)*;* Short Graminoid mix (GSmix); Short Graminoid *Rhynchospora tracyi* (GSrt); Tall Graminoid *Cladium jamaicense* (GTcj); Short (GTcjS) and Tall (GTcjT) ; Tall Graminoid *Typha* (GTt); Bayhead Shrub (SB); Shrub *Salix caroliniana* (Ssc); Tree *Annona glabra* (Tag); Bayhead Trees (TB).
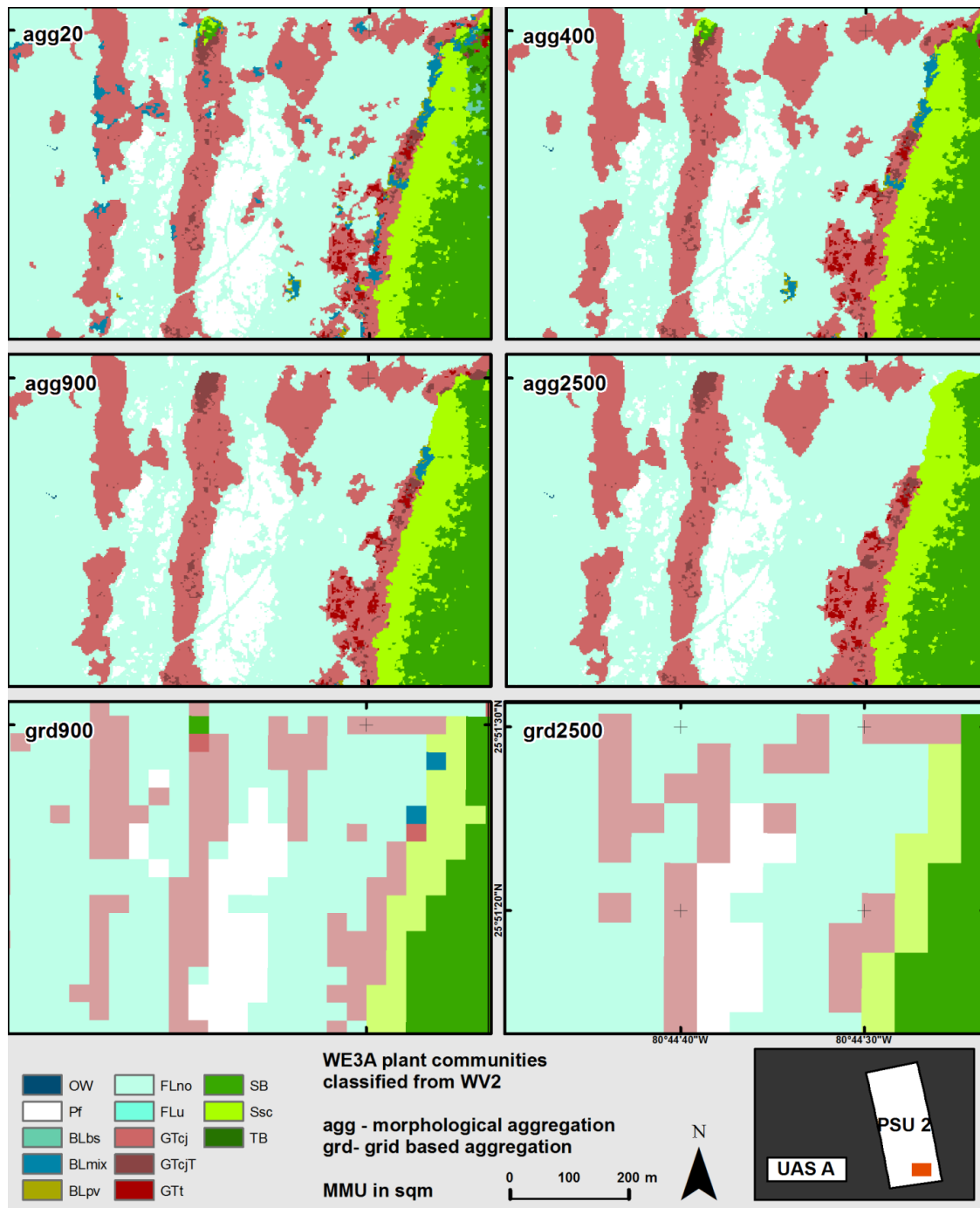
Figure 11. Comparison of morphological aggregation (agg) at 20, 400, 900 and 2500m^2 and grid-based aggregation (grd) at 900m^2 (MMU equivalent to Landsat pixels) and 2500m^2 (MMU equivalent to CERP grids) for a subset of the area south of Tamiami Trail. Classes: Bare Ground peat (BGp); Open Water (OW); benthic Periphyton (Pb); Broad-Leaved *Blechnum serrulatum* (BLbs); Broad-Leaved mix (BLmix); Short Graminoid Broad-Leaved mix (GS BL); Short Graminoid *Eleocharis* (GSe)*;* Short Graminoid mix (GSmix); Short Graminoid *Rhynchospora tracyi* (GSrt); Tall Graminoid *Cladium jamaicense* (GTcj); Short (GTcjS) and Tall (GTcjT) ; Tall Graminoid *Typha* (GTt); Bayhead Shrub (SB); Shrub *Salix caroliniana* (Ssc); Tree *Annona glabra* (Tag); Bayhead Trees (TB).

Figure 12. Comparison of morphological aggregation (agg) method at 20, 400, 900 and 2500m² and grid-based aggregation (agg) at 900m² (MMU equivalent to Landsat pixels) and 2500m² (MMU equivalent to CERP grids) for a subset of the area in western WCA 3A. Classes: Open Water (OW); floating Periphyton (Pf); Broad-Leaved *Blechnum serrulatum* (BLbs); Broad-Leaved mix (BLmix); Broad-Leaved *Peltandra virginica* (BLpv); Floating-Leaved *Nymphaea odorata* (FLno); Floating-Leaved *Utricularia* (Flu); Tall Graminoid *Cladium jamaicense* (GTcj); Tall (GTcjT); Tall Graminoid *Typha* (GTt); Bayhead Shrub (SB); Shrub *Salix caroliniana* (Ssc); Bayhead Tree (TB).
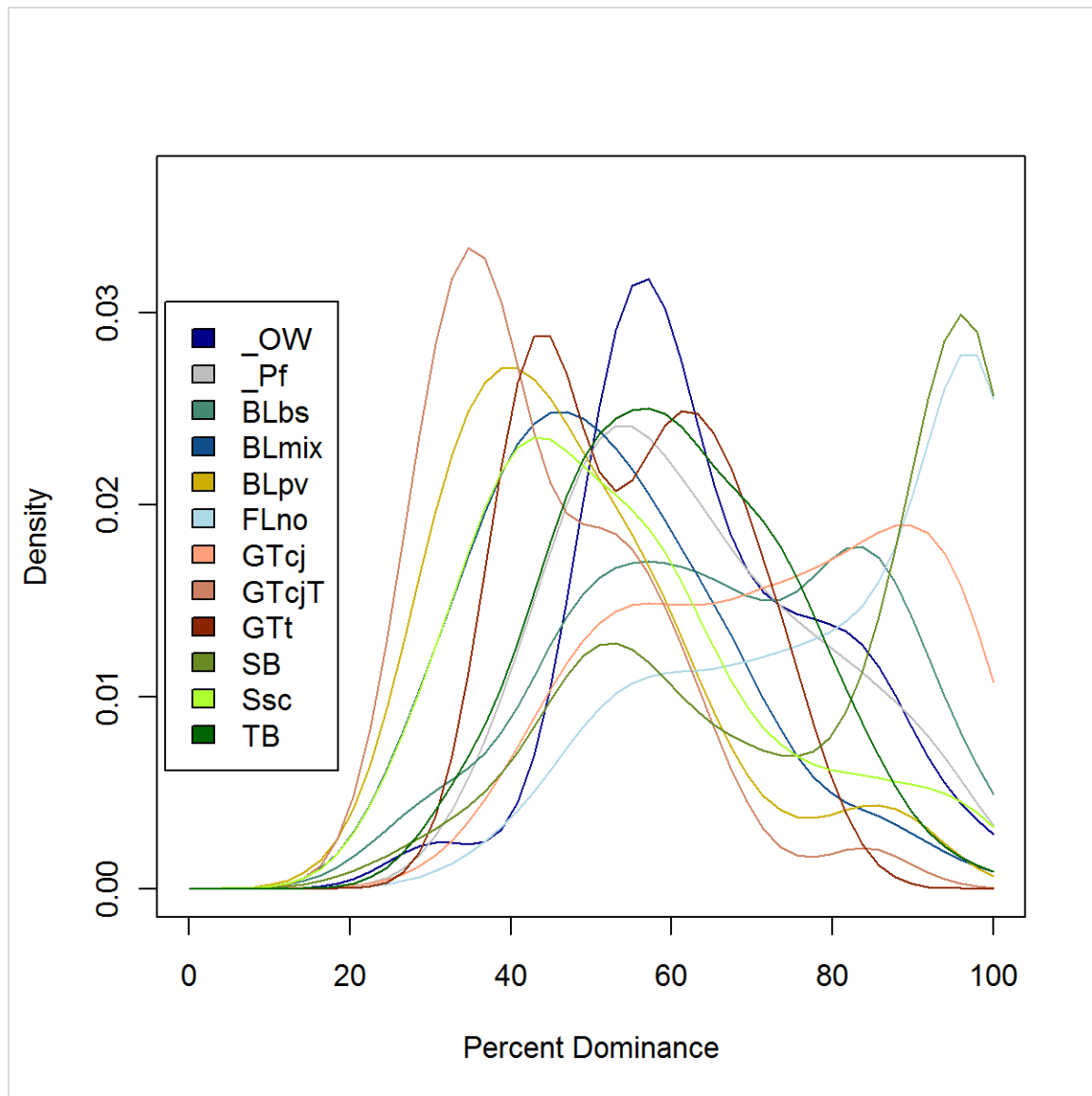
Figure 13. Density of WV2 4m^2 classified community classes within Landsat 900m^2 grid cells in WE3A. Density of grid cells (y-axis) for percent abundance of a class in a cell when it was dominant in the cell (x-axis). Classes: Open Water (OW); floating Periphyton (Pf); Broad-Leaved *Blechnum serrulatum* (BLbs); Broad-Leaved mix (BLmix); Broad-Leaved *Peltandra virginica* (BLpv); Floating-Leaved *Nymphaea odorata* (FLno); Floating-Leaved *Utricularia* (Flu); Tall Graminoid *Cladium jamaicense* (GTcj); Tall (GTcjT); Tall Graminoid *Typha* (GTt); Bayhead Shrub (SB); Shrub *Salix caroliniana* (Ssc); Bayhead Tree (TB).

References

Breiman, L. (2001). "Random Forests." <u>Mach. Learn.</u> **45**(1): 5-32.

Breiman, L. (2002). "Manual On Setting Up, Using, And Understanding Random Forests V3.1."

Chen, X. X., L. Vierling, et al. (2005). "A simple and effective radiometric correction method to improve landscape change detection across sensors and across time." <u>Remote Sensing of Environment</u> **98**(1): 63-79.

Cohen, J. (1960). "A Coefficient of Agreement for Nominal Scales." <u>Educational and Psychological Measurement</u> **20**(1): 37-46.

Cohen, M. J., D. L. Watts, et al. (2011). "Reciprocal biotic control on hydrology, nutrient gradients and landform in the Greater Everglades." <u>Critical Reviews in Environmental Science and Technology</u> **41**(6): 395-429.

Gann, D. and J. H. Richards (2009). Determine the Effectiveness of Plant Communities Classification from Satellite Imagery for the Greater Everglades Freshwater Wetlands &Community Abundance, Distribution and Hydroperiod Analysis for WCA 2A. West Palm Beach, FL, South Florida Water Management District**:** 278.

Hothorn, T., K. Hornik, et al. (2006). "A Lego System for Conditional Inference." <u>The American Statistician</u> **60**(3): 257--263.

Hothorn, T., K. Hornik, et al. (2006). "Unbiased Recursive Partitioning: A Conditional Inference Framework." <u>Journal of Computational and Graphical Statistics</u> **15**(3): 651-674.

Hubert, L. and P. Arabie (1985). "Comparing partitions." <u>Journal of Classification</u> **2**(1): 193-218.

ITT_Visual_Information_Solutions (2009). Atmospheric Correction Module: QUAC and FLAASH User's Guide. Atmospheric Correction Module. Boulder, CO.

Jensen, J. R. (2005). <u>Introductory digital image processing: a remote sensing perspective</u>. Upper Saddle River, NJ 07459, Prentice Hall.

Jones, D., M. Madden, et al. (1999). Vegetation classification system for South Florida National Parks, Draft Report, with addendum by Ken Rutchey and Ted Schall, South Florida Water Management District**:** 14 pp.

Larsen, L. G. and J. W. Harvey (2010). "How vegetation and sediment transport feedbacks drive landscape change in the Everglades and wetlands worldwide." <u>American Naturalist</u> **176**(3): E66-E79.

Larsen, L. G., J. W. Harvey, et al. (2007). "A delicate balance: Ecohydrological feedbacks governing landscape morphology in a lotic peatland." <u>Ecological Monographs</u> **77**(4): 591-614.

Liaw, A. and M. Wiener (2002). "Classification and Regression by randomForest." <u>R News</u> **2**(3): 18-22.

McVoy, C. W., W. P. Said, et al. (2011). <u>Landscapes and Hydrology of the Predrainage Everglades</u>. Gainesville, FL, University Press of Florida.

Nungesser, M. K. (2011). "Reading the landscape: temporal and spatial changes in a patterned peatland." <u>Wetlands Ecology and Management</u> **19**(6): 475-493.

Paolini, L., F. Grings, et al. (2006). "Radiometric correction effects in Landsat multi-date/multi-sensor change detection studies." <u>International Journal of Remote Sensing</u> **27**(4): 685-704.

Rutchey, K., T. N. Schall, et al. (2006). Vegetation classification for south Florida natural areas. Saint Petersburg, Fl, United States Geological Survey**:** 142.

Strasser, H. and C. Weber (1999). "On the asymptotic theory of permutation statistics." <u>Mathematical Methods of Satatistics</u> **8**: 220-250.

USGS. (2010). "Frequently Asked Questions about the Landsat Missions." Retrieved October 24, 2011, from http://landsat.usgs.gov/images_will_work_best_to_fill_in_the_gaps.php.

Vogelmann, J. E., D. Helder, et al. (2001). "Effects of Landsat 5 Thematic Mapper and Landsat 7 Enhanced Thematic Mapper Plus radiometric and geometric calibrations and corrections on landscape characterization." Remote Sensing of Environment **78**(1-2): 55-70.

Watts, D. L., M. J. Cohen, et al. (2010). "Hydrologic modification and the loss of self-organized patterning in the ridge-slough mosaic of the Everglades." Ecosystems **13**(6): 813-827.